Dynamic behavior of ceramic materials

P. Forquin

Chapter 14: Dynamic behaviour of ceramic materials

P. Forquin, Univ. Grenoble Alpes, G-INP, CNRS, Lab. 3SR, pascal.forquin@univ-grenoble-alpes.fr

Abstract

Although the dynamic behaviour of ceramics is less well-known than that of other material families such as metals, polymers, composites or even geomaterials, these materials are nonetheless widely used in many fields under dynamic or shock loading. Under such extreme conditions, these materials exhibit damage and deformation modes that are difficult to observe under static loading. For this reason, the study of their behaviour under high strain-rate is a major challenge. These materials combine low density compared to dense materials like steels with interesting, and even exceptional properties under compressive loadings over a wide temperature range, making them particularly valuable as part of shielding solutions against high-speed impact or high-energy-density pulse loading. On the other hand, these materials exhibit low toughness and ductility in the absence of confinement, which explains their ability to fragment under dynamic tensile loading. In addition, the damage and deformation modes in these materials are particularly sensitive to microstructural parameters such as sintering defects, flaws, grain boundaries, secondary phases. The experimental study of the dynamic behaviour of these materials requires the use of specific experimental methods to characterize their strength under high-rate tension, as well as under high confinement pressure in their pristine (unfragmented) or fragmented states. On the other hand, plasticity and anisotropic damage models must be developed and implemented in numerical codes, considering the influence of loading-rate, level of confinement pressure and deformation or fragmentation state of the ceramic material. This chapter provides a non-exhaustive summary of the work available in the literature on these topics.

14.1 Ceramics used in armour configuration

Armour ceramics made for personal, vehicle or helicopter protections against the treat of small to medium AP (Armour Piercing) projectiles have known a spectacular growth over the last 20 years. Initially made of metallic plates, mostly hard steel, bulletproof systems have evolved since the 1960s to bilayer or multi-layer protective configurations so as to reduce the weight of shielding systems. Composed primarily of alumina ceramic (Al_2O_3) sandwiched between a Doron back plate (a composite of glass-fibre plies), and a polyurethane coating on the front face, such armours halved the weight required to stop a 7.62 mm calibre AP projectile (Barron et al., 1969) (Fig. 1). During the Vietnam war, bilayer configurations were also developed based on hot pressed B_4C as front plate and Kevlar29 as backing for helicopter ballistic seats (Gooch, 2011). The outstanding hardness and compressive strength of ceramics (Bourne et al, 1997; Feng et al, 1998; Forquin et al, 2003a) allow shattering (Madhu et al, 2005) or eroding (den Reijer, 1991) of the bullet during the impact, reducing its penetrative efficiency. Moreover, thanks to their low density (less than half the density of steel materials in the case of silicon carbides), their use allows, for a same ballistic efficiency, a significant weight benefit in comparison with monolithic steel armours (Roberson, 1995).

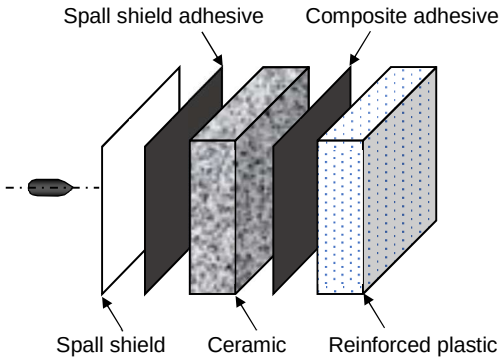

Fig. 1. Exploded view of the composition of early ceramic-based armour configurations. From left to right: debris-repellent liner, adhesive, ceramic plate, adhesive, polymer-matrix composite backing (Barron et al., 1969).

However, the relationship between the mechanical properties of the ceramics and the ballistic performance of the armour configurations still remains difficult to establish. Indeed, during the ballistic impact of an AP projectile, the ceramic plate experiences a complex transient dynamic loading involving, first, a high triaxial state of stress, followed by tensile damage composed of multiple-cracking (possibly due to a spherical divergent wave propagating from the impact point through the target inducing a compression-tensile state) as well as release waves and spalling phenomena resulting from the interaction of release waves. Finally, the debris of the projectile interacts with fragmented media, the resistance of which

depends on the cracking density within the ceramic and the confining pressure exerted by the projectile during the penetration.

A ceramic-based armour configuration analysed by X-ray microtomography after being subjected to the impact of a 7.62-mm API-BZ projectile impact at a speed close to 800 m/s is presented in Figure 2 (Forquin et al, 2022). The two-layer target is made of a Hexoloy® SiC ceramic layer as front face and Dyneema® plate as backing. Dyneema® is a high-performance non-woven composite material which incorporates UHMWPE (ultra-high-molecular-weight polyethylene). The target was placed in a sarcophagus configuration designed to keep most of the fragments in place so the target could be infiltrated and scanned using the micro-X-ray tomography machine in the 3SR Lab with a pixel size of about 60 µm/px. A cut view in the mid-plane of an impacted target is provided in Figure 2. Multiple fractures can be observed in the ceramic and more specifically: radial cracks, circular cracks and Hertzian-cone fracturing emerging on the back side. The ceramic tile is observed to be fully reduced to small debris in its central part. The brightest points correspond to the fragments of the steel projectile core that was shattered on impact. The Dyneema® backing is observed to be strongly deformed but the fragments have penetrated very little. Abundant delamination noted in the composite can be supposed to be a major cause of energy absorption of the kinetic energy of the fragments.

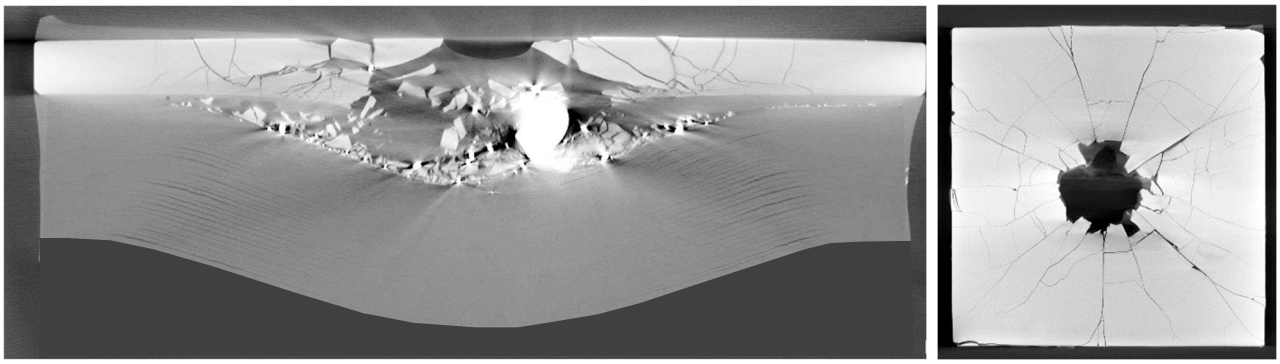

Fig. 2. Target impacted by a 7.62 API-BZ steel core (~800 m/s) and analysed using X-ray microtomography CT (3SR Laboratory) (Forquin et al, 2022).

A large number of ceramic grades have been used as armour materials. Due to their reduced cost compared to other ceramics such as SiC and B_4C alumina-based materials (Al_2O_3) are among the most used ceramics. However, these ceramics suffer from relatively high density (3.90 g/cm^3) and low compression strength and hardness. Among non-oxide ceramics one may mention borides, carbides, and nitrides, such as boron carbide B_4C, silicon carbide SiC, silicon aluminium oxynitride SiAlON, aluminum nitride AlN, titanium diboride TiB_2 and others. In particular, boron carbide is a valuable candidate for lightweight armour given its low density (2.52 g/cm^3) combined with its elevated Vickers hardness (> 30 GPa). Several basic mechanical properties are provided in Table 1 from Reddy et al (2020). RB-SiC and RB-BC are reaction bonding (RB) silicon and boron carbides which correspond to ceramic-metal composites, with a predominant ceramic phase of SiC (RB-SiC) or B_4C (RB-BC). They present very interesting properties for lightweight ballistic protection (Taylor and Palicka, 1974; Hayun, 2017; Dargaud, 2021).

Table 1. Main mechanical properties and relative cost of ceramics for armour application (Reddy et al, 2020).

Property	Al_2O_3	SiC	RB-SiC	B_4C	RB-BC	TiB_2
Density (g/cm^3)	3.9	3.21	3.1	2.52	2.58	4.52
Bending strength (MPa)	310-370	300-400	300-350	350-410	319-415	500-750
Young's modulus (GPa)	300-370	410-480	300-400	400-460	300-350	560
Hardness (GPa)	14-15	24-27	18-20*	30-32	20-22*	26-28
Fracture toughness (MPa.m^{½})	3.5-4.5	2.5-4.5	2.5-4.5	2.5-3.5	5.5-7.9	6.8-7.5
Cost comparison	1	5.3	2	8	4.6	10

* informative values because hardness measurement is not adapted to RB heterogeneous microstructures

14.2 Phenomenology of ceramics under impact

During a ballistic impact, complex successive loadings develop in the ceramic plate leading to extensive damage modes. In the first few microseconds dynamic triaxial compression characterized by very high compression stresses (above the Hugoniot Elastic Limit of the material) occurs beneath the impact point. These high pressures induce micro-plasticity and micro-damage mechanisms, to which may be added the phenomena of amorphization and shear localization (LaSalvia and McCauley, 2010). This damaged zone, usually called the Mescall zone (MZ), is highly comminuted and compacted under the compressive loading by the projectile (LaSalvia et al, 2009). The projectile core experiences erosion or breakage processes and dwells on the ceramic surface without any penetration, thanks to the high hardness of the ceramic.

During the second step, tensile stresses develop in the ceramic plate due to several phenomena such as spherical divergent waves generated upon impact, surface (Rayleigh) waves propagating beneath the ceramic front face, a release

wave coming from the ceramic rear face, and spalling due to the interaction of release waves. Given the low tensile strength of ceramics compared to their compression strength and given also their low toughness, intense fragmentation processes occur in the material which are composed of a high density of oriented cracks initiated at pre-existing flaws such as pores, inclusions, sintering defects at grain boundaries and other heterogeneities (Deng and Nemat-Nasser, 1992; Forquin et al, 2003b; Danzer et al, 2009; Forquin et al, 2021). These processes develop within less than 6-7 µs after impact.

Finally, in the third and final step, the remaining part of the core and debris penetrates into the fragmented ceramic. In that stage, the behaviour of the fragmented ceramic has a strong influence on the penetration resistance of the protective armour system. Penetration can only occur once the ceramic material underneath the projectile has fragmented and if the remaining core debris still has the capacity to move through the ceramic fragments. During this stage, the behaviour of the finely fragmented material is mainly due to its friction, flow and abrasive properties (Shockey et al, 1990). The residual kinetic energy is finally absorbed by plastic deformation of the backing, thus stopping the core and ceramic debris (about 30 to 50 µs after impact).

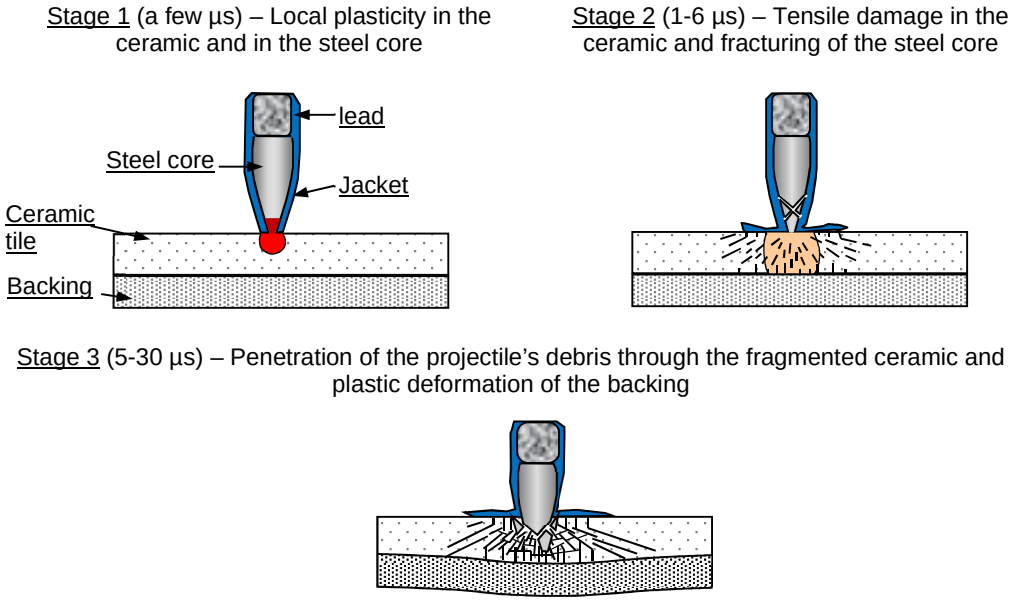

Fig. 3. Three loading stages involving during the penetration process of an AP projectile against a bilayer armour.

From an experimental study performed on transparent armour ceramics (Al_2O_3 and spinel), Krell and Strassburger (2014) concluded that ceramic fragmentation (stage 2) constitutes a major factor governing the armour's ballistic performance as less ceramic fragmentation increases the dwell (flow) time of the projectile on the ceramic surface before its penetration (stages 1 and 2) and coarse ceramic debris has a higher abrasive efficiency (stage 3).

In stage 3, the dynamic stiffness of the backing plays an important role by maintaining a confinement pressure on the fragmented ceramic, making penetration more difficult. However, in stage 1, the Hugoniot Elastic Limit and the confined behaviour of the ceramic are the most important parameters. The Depth-Of-Penetration (DOP) test constitutes a test method to characterize the ballistic efficiency of ceramic tiles in stage 1. The principle of this technique is described in Figure 4. A ceramic tile of thickness (e_{cer}) is fixed to a thick metallic plate. The residual penetration of the projectile into the thick backing plate (P_{al+cer}) is measured post-test. Knowing the depth of penetration of the same projectile impacting at the same velocity the thick metallic plate alone (P_{al}), the ballistic efficiency of the ceramic tile is deduced according to the following equation:

$$\eta = \frac{(P_{al} - P_{al+cer})}{e_{cer}} \frac{\rho_{al}}{\rho_{cer}}, \quad (1)$$

where (ρ_{al}) and (ρ_{cer}) correspond respectively to the densities of the aluminium and ceramic plates. For instance, in order to compare the ballistic performance of four grades of SiC ceramic, DOP-type ballistic tests were carried out with 7.62 mm steel-core (APIB32, V_{impact} = 840 m/s) and tungsten-carbide-core (AP8, V_{impact} = 930 m/s) projectiles (Rossiquet, 2012). The targets consisted of a 4 mm thick front face and a 2024 aluminium alloy backing. Fig. 5 shows the average, minimum and maximum penetration depths observed with the four ceramic grades and the two types of projectile. It can be seen that the SPS-S grade has the best ballistic efficiency against the AP8 projectile. Hexoloy and SPS-L showed similar ballistic performances whereas those of the PS-L grade were less good. Given the mechanical properties of each grade (Table 2) these results confirm a good correlation between ballistic efficiency (Eq. (1)) and ceramic hardness and HEL. However, it should be noted, that the configuration used for the DOP tests is not fully representative of a two-layer armour. Indeed, a rigid rear face (semi-infinite thickness) and lateral confinement favour the confined behaviour of the ceramic before fragmentation (stage 1).

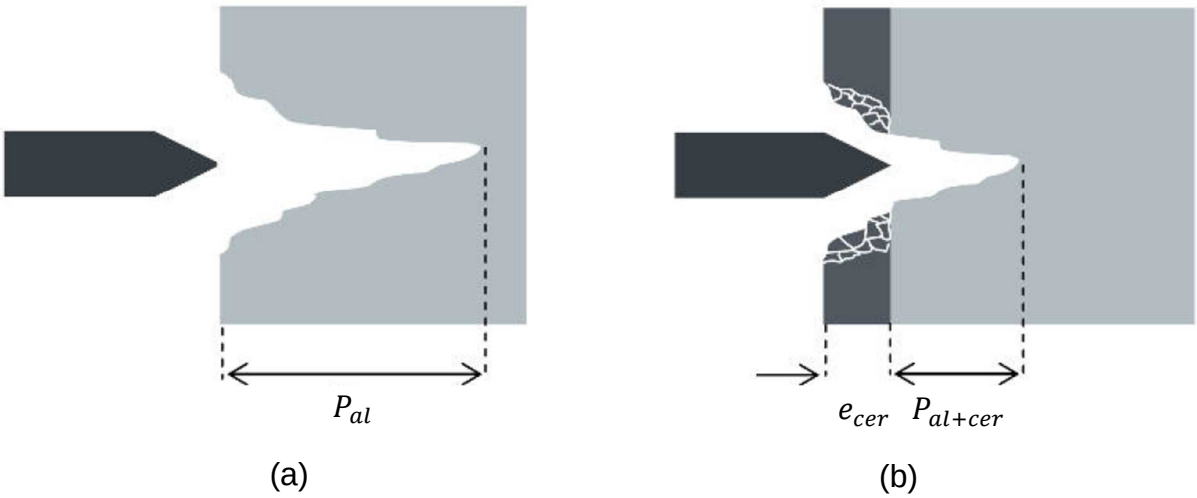

Fig. 4. Schematic representation of the DOP test. (a) Measurement of the penetration of the projectile into the thick backing plate alone. (b) Measurement of the residual penetration of the projectile into the thick backing plate when faced with a ceramic tile.

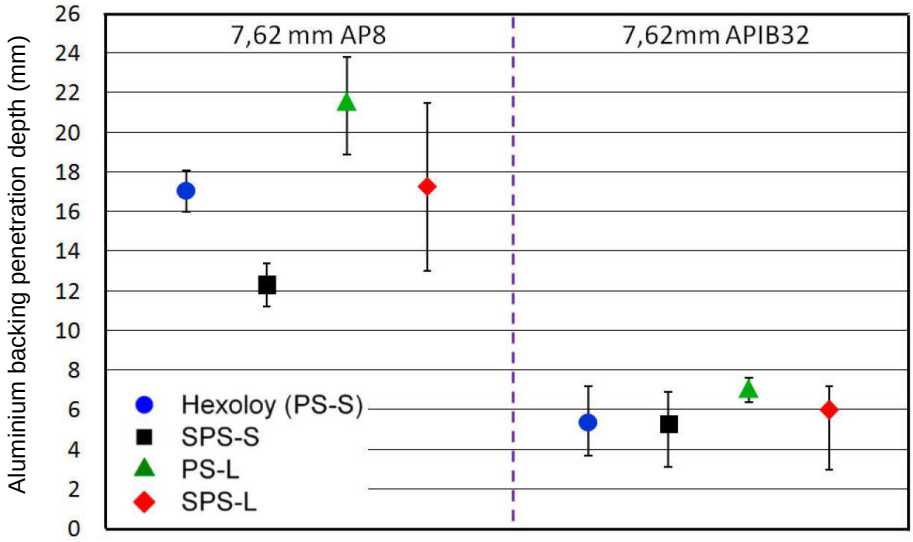

Fig. 5. Average, minimum and maximum observed penetration depths for the four ceramic grades (e_{cer} = 4 mm) and the two projectile types according to Rossiquet (2012).

Tab. 2. Mechanical and microstructural properties of 4 SiC grades (Rossiquet, 2012; Forquin et al, 2018).

Properties \ SiC grades	Hexoloy	SPS-S	PS-L	SPS-L
Sintering type	Solid phase		Liquid phase	
Sintering mode	Natural	SPS	Natural	SPS
Grain size (µm)	6	> 6	3	> 0.5
Hardness HV1 (GPa)	24.3	27	22.2	23.9
Toughness (MPa.m^{½})	3.2	2.5	5.2	3.8
HEL (GPa)	15.1	16.8	7.9	Not measured

In the next subsection, a few studies dealing with the influence of confinement of the ceramic on the penetration process are briefly summarized. The subsequent subsections are dedicated to experimental methods for exploring the behaviour of ceramics under compression loading over a range of strain rates, high-strain rate tensile loading, and the impact properties of fragmented ceramics.

14.3 Influence of confinement on the impact behaviour of ceramic-based armours

In addition to the confinement induced by the backing, several authors have investigated the benefit of front and lateral confinements. According to Sherman and Ben-Shushan (1998), lateral confinement of a few MPa can eliminate the Hertz-

type conical cracking. These authors also concluded it is preferable to choose a backing material of impedance close to that of the ceramic. The effect of frontal confinement has been studied for the case of tungsten rod impacts at impact speeds between 1000 and 2000 m/s. Such tests have shown both positive (Anderson and Morris, 1992) and negative influences (Woodward and Baxter, 1994). In the worst case, the impact of the rod on the front plate (generally made of steel) started to damage the ceramic before the bar was eroded, making the use of this front plate detrimental.

On the other hand, Bless et al (1992) reported a case of quasi-impenetrability for a front face made of hardened steel (Brinell hardness 480) impacted by a tungsten rod at 1400 m/s. According to the authors, this phenomenon occurs thanks to the flow of the projectile along the glue line (2.5 µm thick) separating the front plate from the TiB_2 ceramic. This flow creates a state of confinement on the ceramic in the vicinity of the point of impact, preventing any ejection of debris. This result was confirmed by Malaise (1999), by considering tungsten rods impacting a target made of silicon carbide as front face (thickness = 30 mm) at a speed of 1450 m/s. The pressure exerted by this cylinder on the ceramic in the vicinity of the impact point completely altered the penetration depth of the ceramic (34 mm without the PC cylinder, 3 mm with it). This difference in behaviour can be explained by the high sensitivity of ceramic compressive strength to hydrostatic pressure.

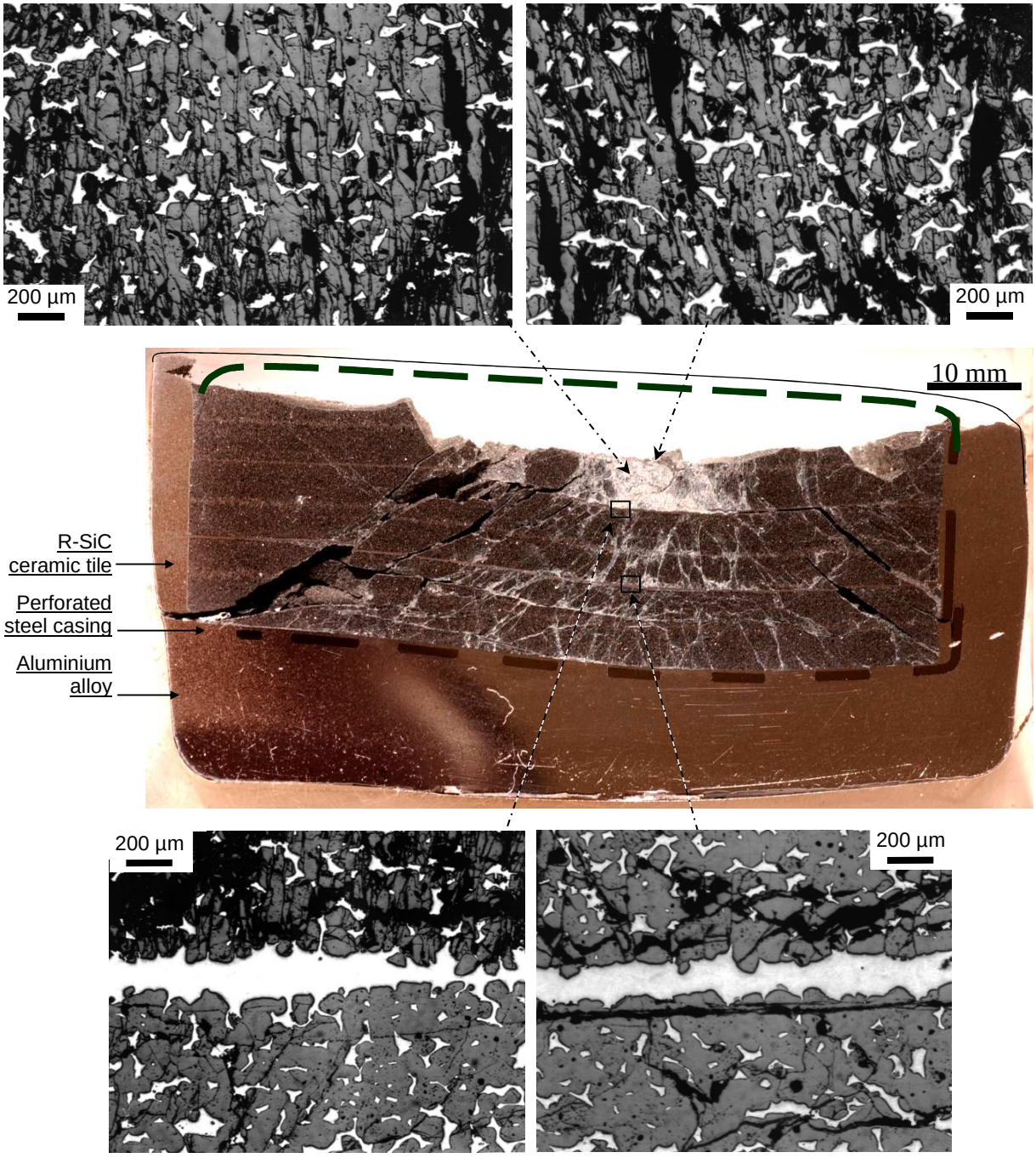

Fig. 6. Impact of an armour-piercing projectile AP 12.7 mm traveling at 880 m/s against a multilayered armour made of three infiltrated ceramic tiles (R-SiC-Al) as front face and aluminium alloy as backing. (Forquin, 2003).

The influence of fragment mobility was also explored using an armour configuration illustrated in Fig. 6. It is made of three tiles of porous ceramic backed with a 15 mm-thick aluminium layer (Forquin, 2003). The porous ceramic was infiltrated through its open porosity with an aluminium alloy to prevent crack opening. A steel casing surrounded the ceramic tiles in order to maintain the three tiles in position during squeeze casting and constrain them during impact. An AP 12.7 mm projectile travelling at 880 m/s impacted the block (Fig. 6). Despite the intense fragmentation consisting of dense and oriented microcracks occurring mainly in the first layer (see the micrographs in Fig. 6), no penetration can be seen even though bending deformation of the target was observed. The residual strength of the ceramic tiles can be attributed to the presence of the aluminium alloy, which ensures cohesion within the material throughout the impact. Edge-on impact experiments performed on non-infiltrated and infiltrated ceramic targets confirm the benefit of metal infiltration on the crack density and also on the residual strength of these materials (Forquin et al, 2003b).

14.4 Ceramics under quasi-static and dynamic compression loadings

14.4.1 Ceramics in uniaxial compression testing at ambient and high temperatures. Comparison with observations made in pyrotechnic spherical expansion tests

One of the most used mechanical tests on ceramics is the quasi-static uniaxial compression test. The difficulty lies in generating high compressive stress (-4 to -8 GPa) while limiting tensile stresses to below the tensile failure strength, which is around ten to twenty times lower than the failure stress in compression for these materials.

Among the numerous experimental data available in the literature, Lankford carried-out extensive experimental campaigns with cylindrical specimens 12.5 mm in length and 6.25 mm in diameter, with perfectly parallel, polished faces. These specimens, made of Lucalox alumina and α-SiC, were loaded at different speeds (Lankford, 1977) and over a wide temperature range (Lankford, 1981).

Tests carried out with alumina show a strong temperature dependency of the compressive strength (Fig. 7). At temperatures below 400°K (region I) and strain rates below 2000 s^{-1}, transgranular axial microcracks were observed with preferred initiation sites located at the intersection between grain boundaries and twins. (Lankford, 1981) Twinning was observed to start from a quarter to half the failure stress, with failure resulting from the coalescence of microcracks. The slight dependence of compressive strength with the strain-rate below 2000 s^{-1} was explained by sub-critical crack growth phenomena previously observed in tension by Evans (1974). By extrapolating the results at 0 K, a compressive strength independent of the loading rate was predicted ($\sigma_c^{(T=0)}$ = 4075 MPa).

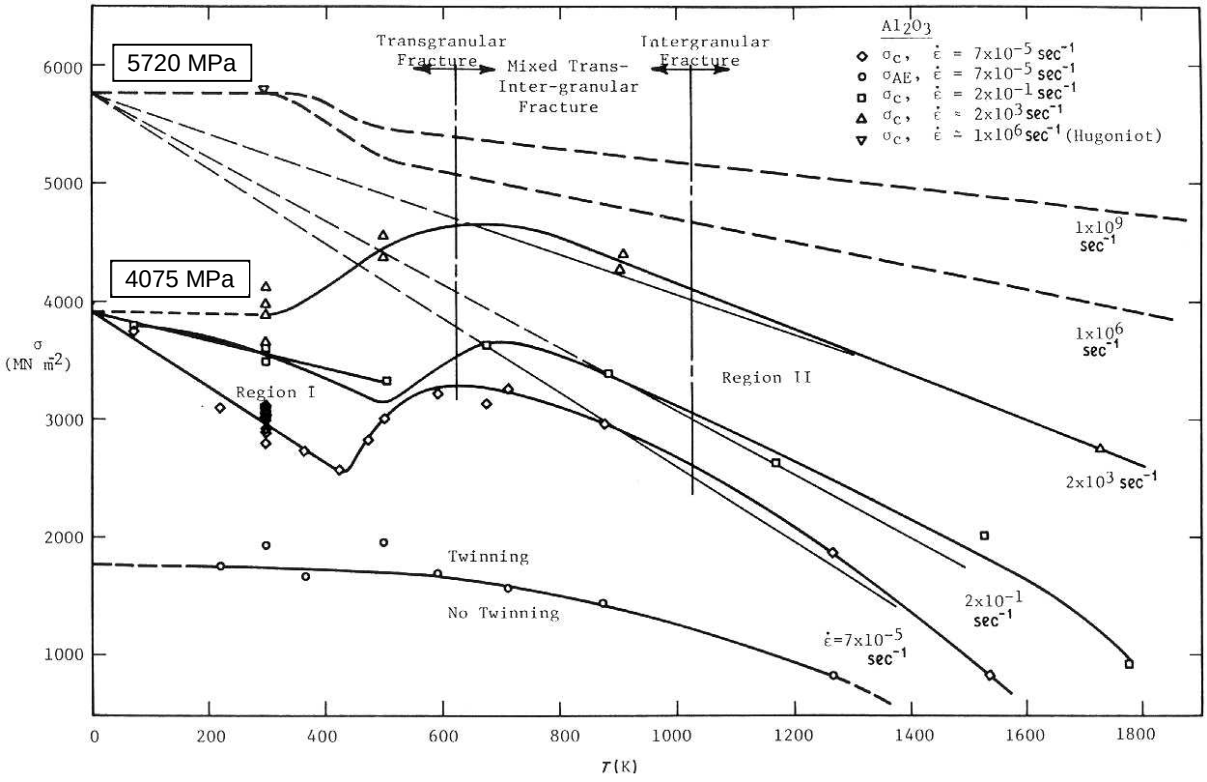

Fig. 7. Quasi-static uniaxial compression strength of alumina as a function of temperature (Lankford, 1981).

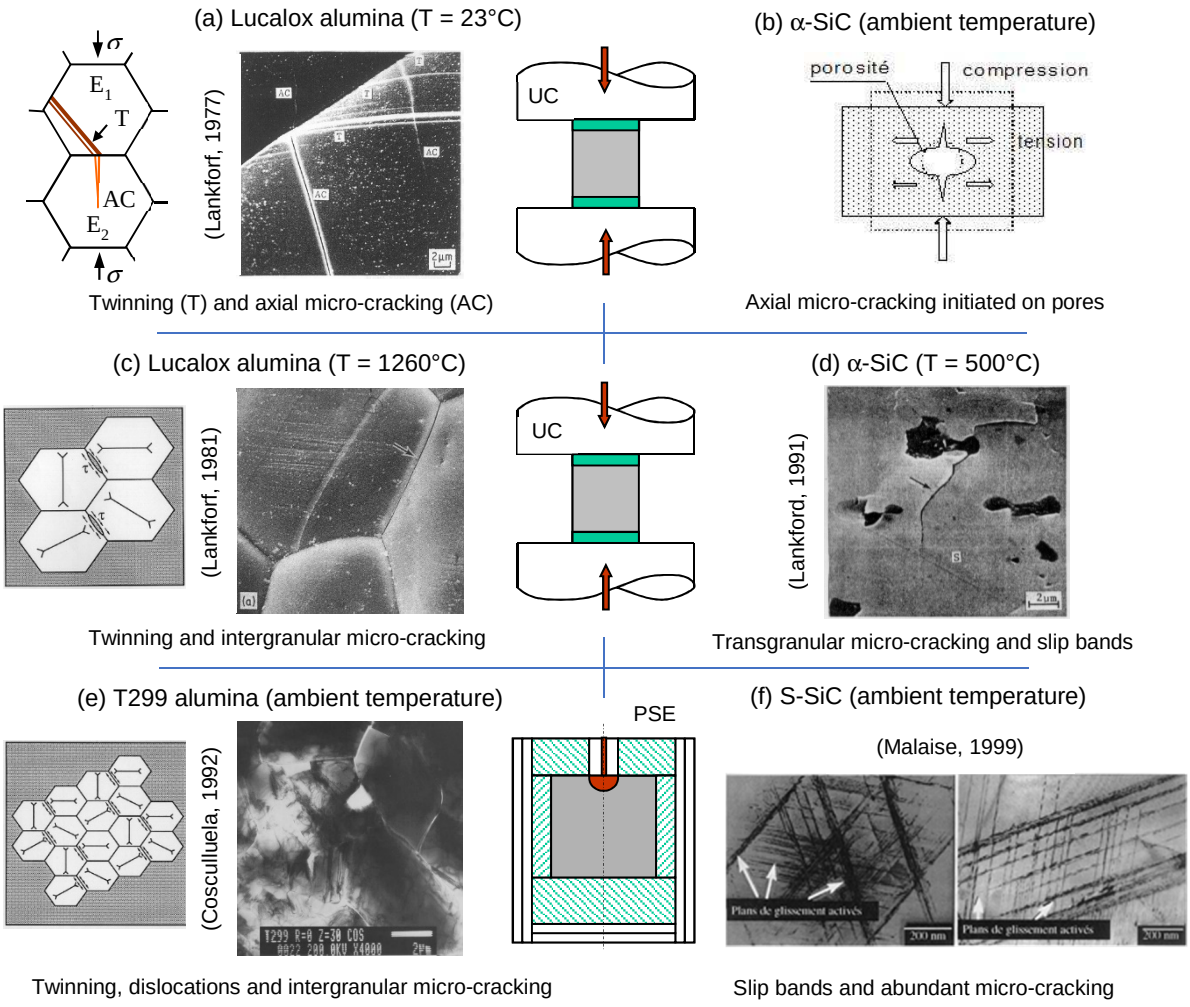

Fig. 8. Microplasticity and microcracking mechanisms observed in alumina and SiC ceramics under uniaxial compression (UC) test at ambient and elevated temperature and in pyrotechnic spherical expansion test (PSE) at ambient temperature. Figure derived from Forquin (2003) with illustrations from Lankford (1977; 1981; 1991), Cosculluela (1992) and Malaise (1999).

At high temperatures (above 1000 K), intergranular microcracking was observed in alumina samples whose compression strength rapidly decreased with temperature (region II). Failure was caused by the coalescence of microcracks present at grain boundaries (Fig. 8c). Extrapolation of the curves obtained at high temperature (T > 1000 K) again gives a single point (Fig. 7) at T = 0 K independent of the loading rate ($\sigma_c^{(T=0)}$ = 5720 MPa), which is not far from the yield strength deduced from plate impact tests (Munson and Lawrence, 1979). This analogy between high temperature and high strain-rate is also highlighted by the failure patterns observed in pyrotechnic spherical expansion (PSE) tests applied to two alumina ceramics (fine-grained T299 and coarse-grained AL23) which showed intense cracking at grain boundaries (Fig. 8e), coupled with abundant microplasticity activity (Cosculluela, 1992, cf. chapter 4). The damage mechanisms present at high temperatures or high rates therefore seem to coincide for alumina.

Lankford (1981) also studied the compressive strength of α-SiC at different temperatures (0°C < T < 800°C). Whereas, the compression strength was weakly sensitive to temperature below 600°C, a drop of compression stress was observed above 600°C, accompanied by a change in fracture mode from transgranular below this temperature (Fig. 8b) to totally intergranular above. Slip bands were also noted at 500°C and above (Fig. 8d). While transgranular cracking is attributed to the activation of pre-existing defects, intergranular cracking is justified by localized slip or microplasticity at grain boundaries, as was also observed in pyrotechnic spherical expansion tests conducted by Malaise (1999) (Fig. 8f). As with alumina, the failure stress/temperature curve available between 600 and 800°C was extrapolated to a temperature of 0 K for which a compression stress of 10.5 GPa was deduced. This prediction is very close to the yield strength (10.9 GPa) obtained in plate impact tests (Cagnoux et al., 1987; Bourne et al., 1997) on S-SiC grade which is also a ceramic obtained by natural sintering (Table 3).

Tab. 3 Compression strength of different SiC grades provided by plate-impact tests and uniaxial compression tests

Test	Grade	Reference	$\|\dot{\varepsilon}\|$ (s^{-1})		
1D-strain loading				HEL (GPa)	σ_y (GPa)
Plate impact	S-SiC	(Cagnoux et al., 1987) (Bourne et al., 1997)	> 2000	13.5 13.5	10.9 10.9
	SiC-B	(Kipp and Grady, 1990) (Bourne et al., 1997)	> 2000	14.8-15.3 15.7	12.0-12.4 12.5
1D-stress loading				Geometry	σ_C (GPa)
Uniaxial compression test	α-SiC	(Lankford, 1981) (Dunlay et al., 1989)	< 100	Cylindrical Diabolo	4.0 4.55
	S-SiC	(Bourne et al., 1997) (Forquin et al, 2003a)	10^{-3}	Diabolo	5.21 6.7
	SiC-B		10^{-3}	Diabolo	5.15 5.8
SHPB dynamic UC test	S-SiC	(Bourne et al., 1997)	600	Diabolo	7.47
	SiC-B				8.17

HEL: Hugoniot Elastic Limit, σ_y : Yield strength, σ_c : strength in uniaxial compression

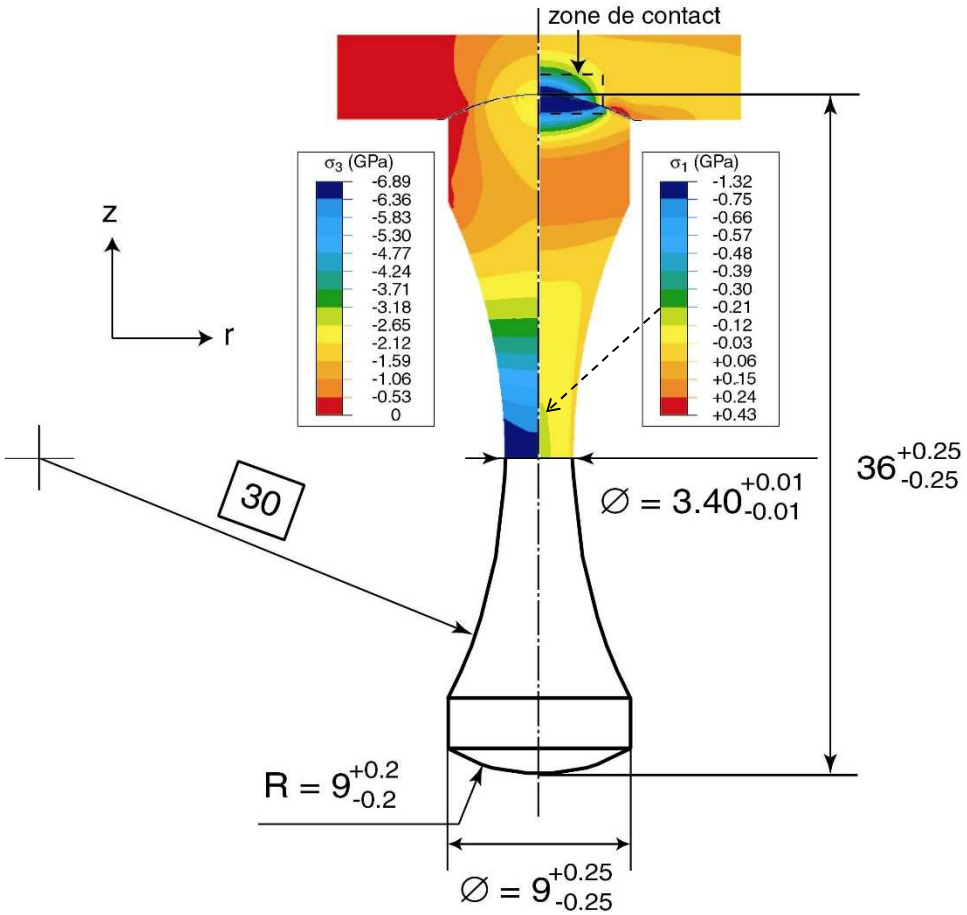

Fig. 9. Geometry of diabolo sample considered in Forquin et al (2003a). Top view: Fields of 1st and 3rd principal stresses. Bottom view: sample dimensions.

However, the cylindrical geometry has the disadvantage of generating a non-homogeneous and non-uniaxial stress state due to the friction generated at the anvil-specimen interfaces. In addition, the anvils must withstand very high stresses and resist being damaged when the ceramic sample breaks, which raises some difficulties for the strongest ceramics. Diabolo

(or “dog-bones”) geometries (Fig. 9) make it possible to circumvent these difficulties. This type of geometry was used in particular by Dunlay et al. (1989), Bourne et al. (1997) and Forquin et al (2003). The geometry implemented by Forquin et al (2003a) as well as the stress fields associated with the first and third principal stresses calculated using the Abaqus FE code are presented in figure 9. The radial stress at the level of the ligament (narrowest section of the toroidal part of the specimen) is negative and about 50 times lower than the axial stress, thus ensuring a quasi-uniaxial state of stress. In addition, the diabolo geometry ensures a state of stress at the level of the ligament that is independent of the contact conditions. The contact surface between the anvil and the spherical geometry specimen strongly limits the amplitude of the tensile stresses (figure 9). This specimen geometry provided a compressive strength for the S-SiC ceramic of 6.7 GPa (Forquin et al, 2003a). However, a probabilistic analysis showed that the initiation of the fracture could be influenced by surface defects (roughness). In conclusion, the uniaxial compression test performed on ceramics remains a delicate and difficult-to-interpret technique for identifying the parameters of a constitutive model. Dynamic uniaxial compression tests were conducted with SHPB facilities, showing a significant increase of strength with strain-rate (Table 1). However, its interpretation remains uncertain as this increase of strength could be explained, at least in part, by a component of confinement resulting from inertial effects.

14.4.2 Ceramics in triaxial compression testing

Triaxial compression testing is an alternative way of attempting to characterize the plastic behaviour of ceramics under confinement. In the first stage, hydrostatic pressure is applied to the sample by means of a confining fluid. This pressure is then kept constant and an axial loading is added to the hydrostatic loading. Deviatoric stress (corresponding to the difference between axial stress and radial stress held constant in the second stage) can be plotted as a function of the axial compression strain. Figure 10 shows the evolution of the deviatoric stress in a BeO polycrystal manufactured by hot pressing (Heard and Cline, 1980). A transition from brittle failure at atmospheric pressure to a ductile response is noted when the confining pressures exceed 0.5 GPa. While the failure pattern is characterized by axial or inclined cracking without confinement, the authors noted that under high pressure, these cracks disappear and are replaced by intragranular slip bands favoured by the stacking of dislocations at grain boundaries. The maximum deviatoric stress can be plotted as a function of the confining pressure. The envelop curve plotted for different kinds of ceramics in Fig. 10b shows a sharp rise in the deviatoric resistance as a function of pressure, which could be considered in a constitutive model of the tested ceramic. However, these triaxial tests are generally limited to static loading and to confining pressures not exceeding about 1 GPa, which limits their interest in identifying the mechanical behaviour of ceramics subjected to high-speed ballistic impact loading.

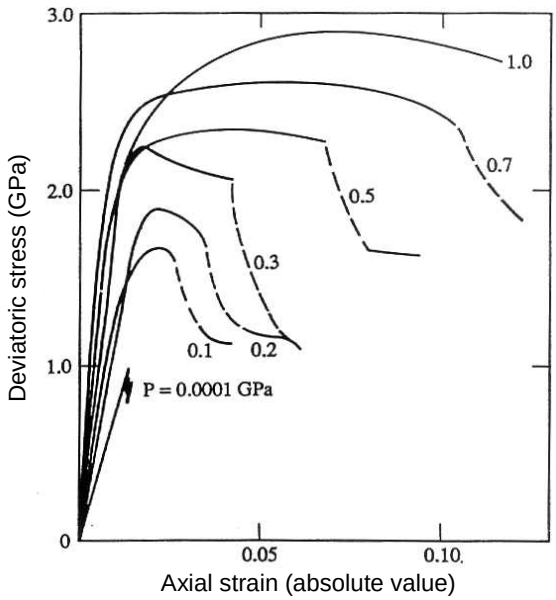

a – Deviatoric stress as a function of axial strain for different lateral pressures (in GPa) in a hot-pressed BeO polycrystal

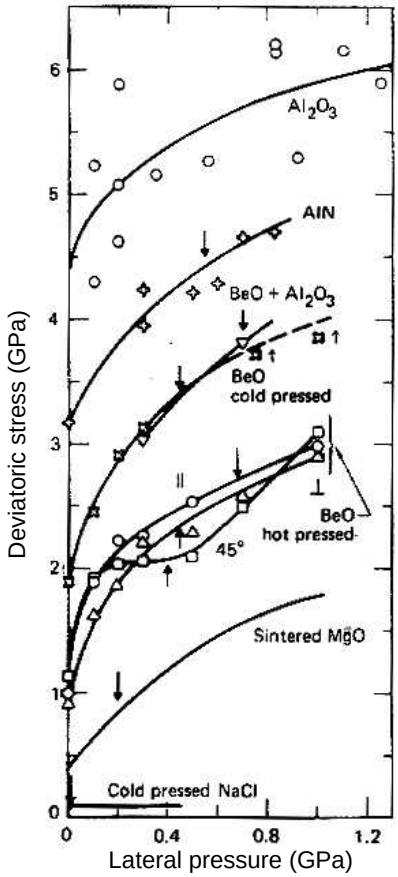

b – Effect of lateral pressure on the maximum deviatoric stress for different ceramics (the brittle/ductile transition is indicated by solid arrows)

Fig. 10. Results of triaxial compression tests performed on different kinds of ceramic (Heard et Cline, 1980).

14.4.3 Ceramics in normal plate-impact testing

Planar, normal, parallel, impact (or normal plate-impact) implies that two parallel and flat surfaces come into contact and the direction of motion of the projectile is perpendicular to its surface (in contrast with inclined impact). Prior to impact, the projectile was travelling at a velocity V_{impact}, and the target was at rest. After impact, two compressive shock waves are created, one travelling into the target and one travelling into the projectile. All points located sufficiently far from the periphery of the striker and target plates were subjected to uniaxial strain-loading. By considering the conservation of mass and momentum a relationship can be built between the EOS (Equation Of State) of each material (flyer and target plates) and the final state of pressure and particle velocity prior the arrival of release waves from rear free surfaces (see for instance (Meyers, 1994)).

Normal plate impact tests are usually instrumented with a laser interferometer, such as VISAR or PDV, providing the particle velocity profile related to the target (ceramic) rear face. When the elastic limit under the imposed stress and strain-rate conditions is reached, a change of slope is noted that corresponds to the so-called Hugoniot-Elastic-Limit (HEL) (Fig. 11).

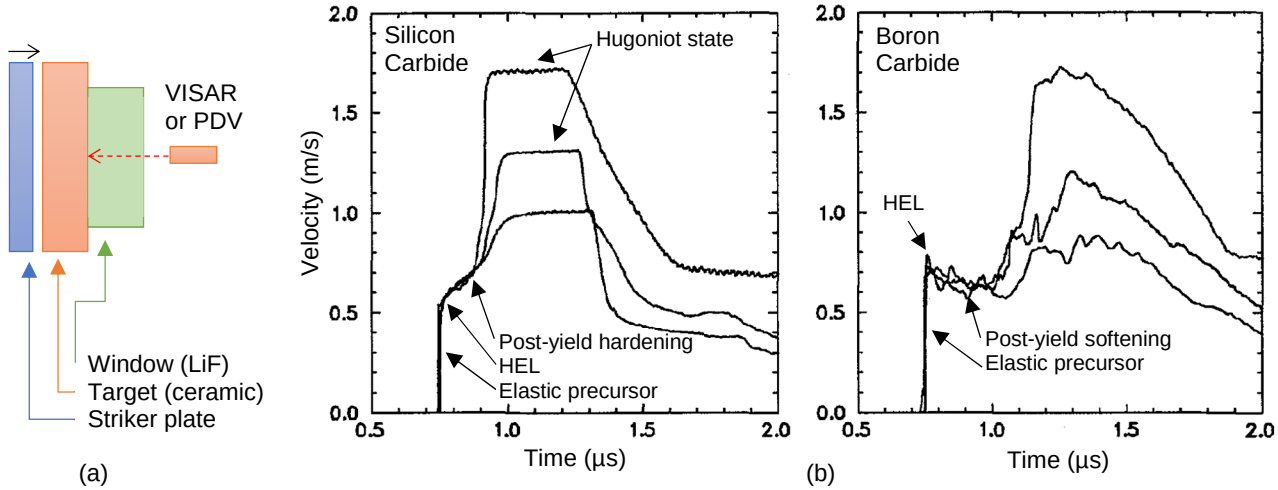

Fig. 11. (a) Principle of normal plate-impact. (b) Shock and release wave profiles for silicon carbide and boron carbide ceramics measured with velocity interferometry diagnostics (Grady, 1994).

The HELs calculated by the impedance matching method are about 15-16 GPa for the silicon carbide and 18-20 GPa for the boron carbide considered in Grady (1994). The HEL corresponds to a non-elastic response of the material at the macroscopic scale and can result from microplasticity activity (Cosculluela, 1992) or damage (micro-cracking) mechanisms (Rosenberg et al., 1987). By considering a Tresca or Huber-von Mises criterion, a yield strength corresponding to the axial yield stress in a uniaxial stress state can be deduced from the HEL (which corresponds to the axial stress of yielding in uniaxial strain state) using the following equation:

$$\sigma_{yield} = \frac{1-2\nu}{1-\nu}\sigma_{HEL} \quad , \tag{2}$$

where ν is the Poisson's ratio of the tested material. The values of HEL and elastic limit (σ_{yield}) of two SiC ceramics are reported in Table 1.

Regarding the post-yield characteristics of the precursor waves, they appear dramatically different for the two materials shown in Fig. 11b. In the case of silicon carbide, the positive slope of the precursor wave reveals a subsequent hardening due to a significant resistance to dislocation plasticity or compressive shear fracture that persists in silicon carbide as the dynamic shear deformation in the shock process proceeds (Grady, 1994). By contrast, in boron carbide, precursor waves indicate post-yield stress softening. Stress relaxation suggests a rate-sensitive deformation process, probably accompanied by precursor attenuation with propagation distance.

The use of piezoresistive pressure gauges in plate impact testing can provide access to lateral and axial stress profiles in the target so the equivalent stress (Huber-von Mises equivalent stress) can be deduced:

$$\sigma_{eq} = 2\tau = |\sigma_x - \sigma_y| \tag{3}$$

Figure 12 illustrates the experimental results obtained by Bourne et al. (1997) with two SiC ceramics in the experimental configuration depicted on Fig. 12a. The HEL of both ceramics is deduced from the change of slope in the axial stress profile ($HEL_{S\text{-}SiC}$ =13.5 GPa, $HEL_{SiC\text{-}B}$ =15.7 GPa). In the first stage (lasting approximately 0.3 µs), an increase in shear strength with the shock level is observed for both SiCs. However, in the second stage, the authors observed a drop in the

equivalent strength of S-SiC as the lateral stress increased (Fig. 12b). In addition, the higher the shock level reached, the higher the drop of equivalent strength (Fig. 12c). Conversely, the equivalent strength of SiC-B decreased much less with time. The authors attributed the loss of shear strength of S-SiC above the HEL to Mode II cracking of the material, made possible by the microplasticity generated at the HEL, which is confirmed by the lack of spalling (tensile) strength measured in the same test. Compressive damage within the ceramics is therefore likely, even if its link to the HEL is difficult to demonstrate.

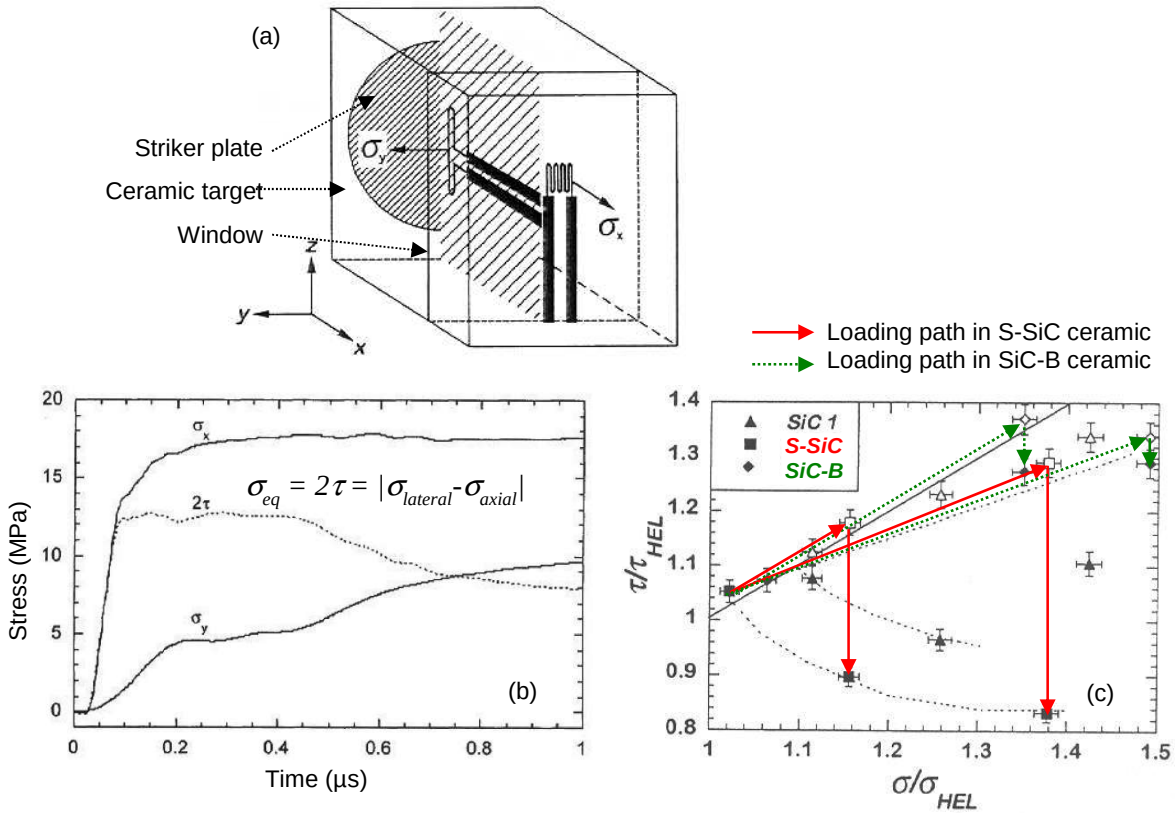

Fig. 12. Plate-impact experiments performed on two SiCs with pressure gauge measurements (Bourne et al., 1997) (a) Principle of plate impact with pressure gauges, (b) Stress profiles, (c) Normalised shear stress as a function of shock stress normalised by the HEL with $HEL_{S\text{-}SiC}$ =13.5 GPa, $HEL_{SiC\text{-}B}$ =15.7 GPa (empty symbols correspond to the start of each test, while solid symbols correspond to the stresses present at the end of the test).

14.4.4 Ceramics in quasi-isentropic compression testing

Normal plate-impact experiments allow the determination of the pressure-volume-energy response of a material along a path referred to as the Hugoniot. However, in many applications, the loading paths differ from the Hugoniot and are closer to isentropic loading (Lindl, 1995). Testing facilities such as the Z-machine at Sandia National Laboratories and GEPI at CEA-Gramat (France) allow the Isentropic Compression Experiment (ICE) to be conducted. The GEPI machine is based on High Pulsed Power (HPP) technologies. This generator applies the strip line concept (Mangeant et al, 2002): two electrodes, separated by dielectric foils and locally connected by a short circuit (Fig. 13a) are subjected to an intense current. In GEPI experiments, the current reaches a maximum intensity of 3.3 MA in about 0.5 µs. The resulting Laplace-Lorentz forces are applied to the internal face of the electrodes. The corresponding pressure pulse applied to the electrode can be directly assessed knowing the time evolution of the current *I(t)*, the width of the terminal part of the electrode *W*, the vacuum permeability μ_0 and a coefficient factor k_p (close to 1) that is related to edge effects in the strip line.

$$\sigma_{mag}(t) = k_p \frac{\mu_0}{2}\left(\frac{I(t)}{W}\right)^2 \quad (4)$$

This ramp loading generated by the GEPI machine allows isentropic compression experiments to be conducted on specimens placed on the electrode. During the experiments, a compressive pulse propagates through the electrodes and the ceramic specimens before reaching the LiF windows (Fig. 13a). Given the symmetry of the tested configuration (Fig. 13a), two samples of different thickness can be tested during a single GEPI compression test, so a Lagrangian analysis method can be applied to the data. This method, based on the integration of the equations of conservation of mass, momentum and energy, does not need any assumptions to be made about the behaviour of the material (Cagnoux et al., 1987). The principle is based on a comparison of velocity signals obtained on two different thicknesses of a material (Fig. 14a). For each particle velocity u_p, the corresponding wave speed $C_L(u_p)$ is calculated. Once the relation $C_L(u_p)$ is known,

it is possible to compute increments of longitudinal stress σ_x, longitudinal strain ε_x (stress and strain being negative in compression) or specific volume associated with each increment of velocity as follows:

$$\sigma_x = -\rho_0 C_L(u_p) du_p \tag{5}$$

$$dv = -\frac{1}{\rho_0 C_L(u_p)} du_p \tag{6}$$

$$d\varepsilon_x = -\frac{du_p}{C_L(u_p)} \tag{7}$$

Two methods can be used to determine the HEL of the material. The first consists in determining the velocity at which a slope change is observed in the velocity profile (i.e. u_{HEL} = 600 m/s in Fig. 8). This value can be converted to stress. The second consists in exploiting directly the results of Lagrangian analysis to assess the elastic limit. Both methods lead to a HEL of 16.8 GPa for this silicon carbide.

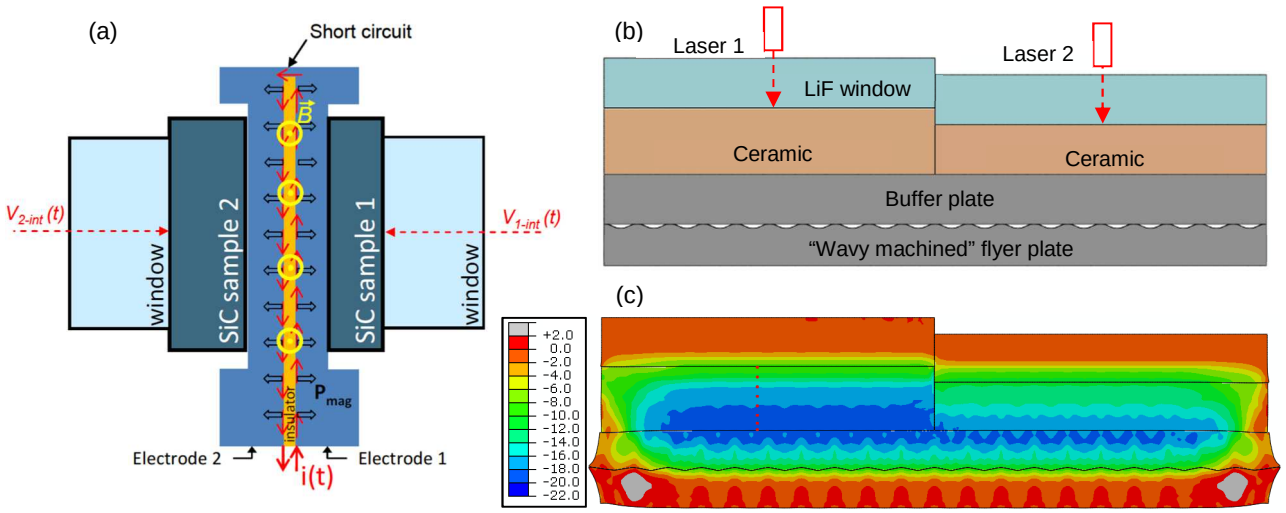

Fig. 13. Two experimental configurations used to perform compression tests which allow the use of Lagrangian analysis. (a) The GEPI facility (CEA-Gramat). (b) The shockless plate-impact configuration based on the wavy-machined flyer plate technique proposed in the 3SR Lab. (Grenoble).

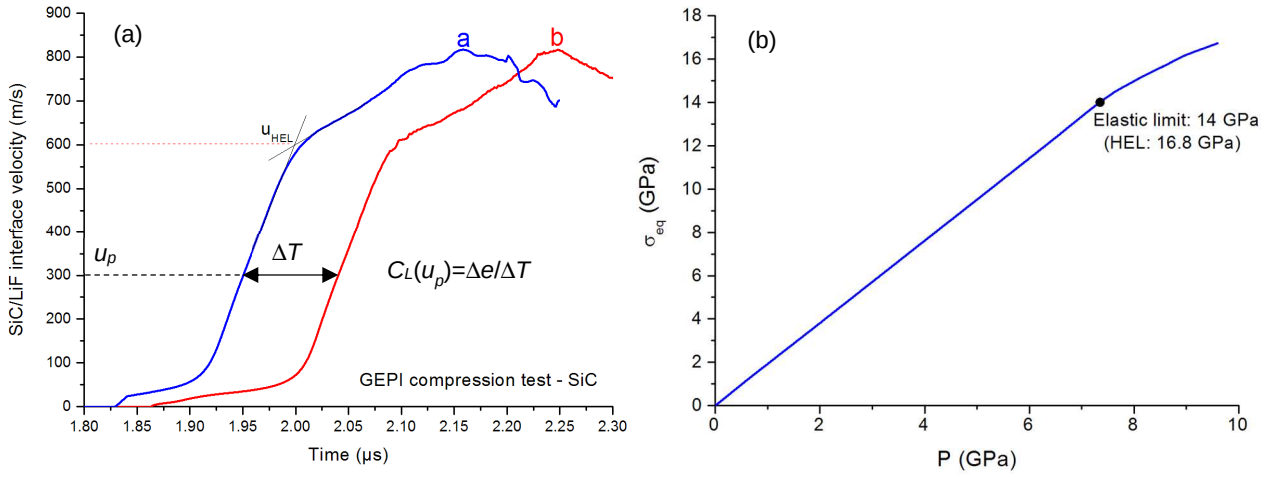

Fig. 14. Data processing GEPI compression test on two SiC specimens. (a) Velocity signals measured on two specimens with thicknesses e = 3 and 4 mm (arbitrary origin of time). (b) Obtained response in terms of equivalent stress versus pressure.

The longitudinal stress obtained using Lagrangian analysis is not sufficient to determine the equivalent stress. Nevertheless, given that in triaxial loading ($\sigma_y = \sigma_z$) the equivalent stress can be deduced by knowing the hydrostatic pressure:

$$\sigma_{eq} = \frac{3}{2}(-\sigma_x - P) \tag{8}$$

By setting an equation of state for the SiC material, one can thus evaluate the evolution of the equivalent stress. In the case of this silicon carbide grade, a very low variation of the *K+(4/3)G* modulus is observed during the elastic compression and a constant bulk modulus K can be assumed ($P = K.\varepsilon_x$) . The axial strain and axial stress being known (Eqs. 4 and 6), the equivalent stress in the ceramic sample during the compressive loading is deduced (Eq. 7). The equivalent stress/pressure curve deduced from the GEPI experiment is presented in Figure 9. The non-linear part of this curve can be directly used to identify the pressure-dependent plasticity model for ceramics (e.g. the Johnson-Holmquist model).

However, the ICE experiments based on High Pulsed Power (HPP) technologies suffer from several inconveniences such as the limited size of the electrodes in order to reach a high level of pulsed pressure, the cost of the equipment and operating costs. It is the reason why a novel experimental approach was proposed by Forquin and Erzar (2017) to generate ramp loading. It is based on the use of a standard plate-impact facility along with wavy-machined flyer plates that can be produced by chip-forming (Fig. 13b). In this experimental configuration the target is composed of a buffer, the role of which is to homogenize the stress field in the transverse direction of the sample, two ceramic samples of different thickness each backed with a window plate. Finally, shockless compression loading having been applied to the sample, Lagrangian analysis of the data is made possible, so the axial stress/strain response of the brittle sample material can be calculated. Although this technique has been numerically validated, its practical use is still under development in the 3SR Laboratory (Grenoble).

14.4.5 Synthesis: Experimental methods to characterise the compressive response of ceramics

A short summary of the main experimental methods used to characterise the compressive behaviour of ceramics at high strain rates is presented in Fig. 15 and their main advantages and drawbacks are listed in Table 4. As previously explained, the uniaxial compression test conducted on ceramics constitutes a delicate and difficult-to-interpret technique as the results can be influenced by contact conditions (cylindrical samples), induced tensile stresses (diabolo samples, roughness defects), confinement resulting from inertial effects (SHPB tests). Although triaxial compression testing constitutes a very interesting technique to characterise the brittle-ductile transition and the damage and micro-plasticity mechanisms involved as a function of the level of pressure, it is limited to static loadings and to confining pressures not exceeding about 1 GPa, which is a serious limitation in the case of armour ceramics.

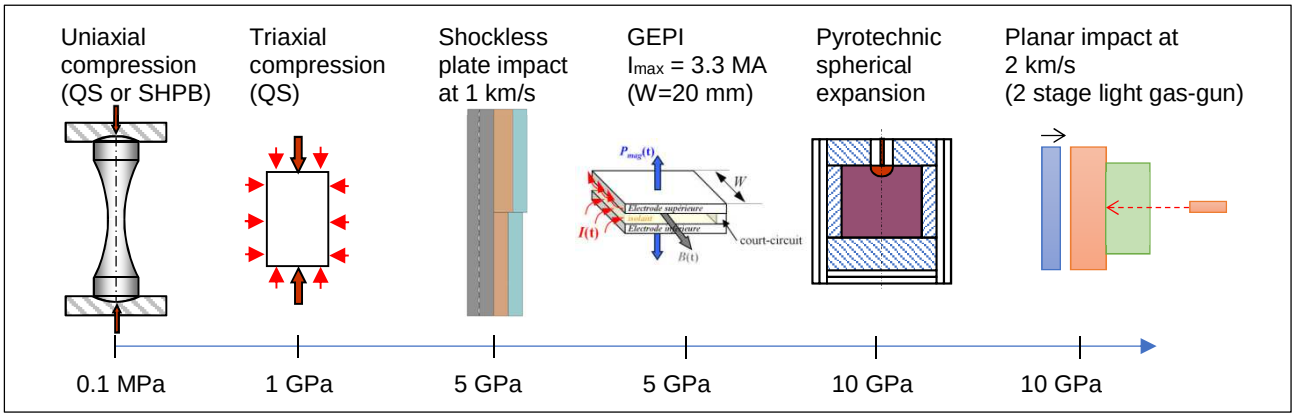

Fig. 15. Order of magnitude of the radial stress reached in samples subjected to various loading conditions.

Table. 4. Some advantages and drawbacks of testing methods use to characterize the compression behaviour of ceramics.

Techniques	Advantages	Drawbacks
QS and dynamic uniaxial compression	Std mechanical press or SHPB apparatus	- Failure due to tensile stresses and surface flaws - Not representative (no confinement, low strain-rate)
Triaxial compression	Investigation of brittle-ductile transition	- Difficult to perform at high pressure - QS loading
Normal plate-impact	Measurements of HEL, Possible use of stress gauges	- Non-controlled strain-rate - No direct measurement of stress-strain relation
GEPI and other HPP	Lagrangian analysis, Stress-strain relation	- Single rise time, limitation of pressure level - Limited plastic strain and pressure
Shockless plate-impact	Lagrangian analysis, controlled strain-rate	- Limitation in the impact speed - Technique still under development
Pyrotechnic spherical expansion tests	Analysis of micro-plasticity and damage modes by TEM and SEM	- Short pulse duration - No direct identification of constitutive laws

Planar impact experiments provide a characterization of the Hugoniot elastic limit and of the Hugoniot state at very high pressure. However, the level of strain-rate is not well controlled and this test only gives access to the final state. Conversely, High Pulsed Power (HPP) technologies such as the GEPI machine allow Isentropic Compression Experiments (ICE) to be conducted. Given the symmetry of the test configuration two samples of different thickness are loaded with the same ramp so Lagrangian analysis can be applied to the data. The shockless plate-impact configuration based on the use of a standard plate-impact facility along with wavy-machined flyer plates that can be produced by chip-forming allows researchers to benefit from some of the advantages of the 2 previous techniques but is still under development. Finally, the pyrotechnic spherical expansion method gives the opportunity to impose a loading path that could be more representative of a ballistic impact (spherical divergent wave) (Cosculluela and Forquin, 2022). However, it remains problematic to use in view of the difficulty of identifying a constitutive behaviour law.

14.5 Ceramics under tensile loadings

Several experimental techniques are currently employed to characterise the tensile strength of ceramics. For instance, Brazilian tests (diametral compression of a disc) can be performed with a Split Hopkinson Pressure Bar apparatus. However, this technique is limited to quite low strain-rates (about a few tens of s^{-1}) when applied to ceramics. Indeed, the limited loading-rate results from the long rise time of loading (more than tens of µs) that needs to be applied to the sample to ensure a correct mechanical equilibrium of the sample. For instance, typical stress-rates ranging from 3 to 6 GPa.s^{-1} were reached in Brazilian tests applied to alumina samples by Chen et al (2014) and by Scapin et al. (2017) leading to a single fracture in each tested specimen. By contrast, the edge-on impact technique and spalling produced by plate-impact or by pulsed-power technology provides much higher strain-rates. Their principal advantages and drawbacks are briefly summarised in the next subsections.

14.5.1 The edge-on impact test

The Edge-On-Impact (EOI) experimental method constitutes a simple and easy test method to investigate the fragmentation process in ceramics at high-strain-rates (Forquin and Cosculluela, 2022). It relies on the following principle: a metallic cylindrical projectile hits the edge of a rectangular tile whose thickness is generally smaller than the projectile diameter. The compressive strength of ceramics being about ten to twenty times higher than their tensile strength, a large range of impact velocity can be considered to generate tensile damage at various loading-rates without inducing any compressive damage near the impact point. The loading, of triaxial shape in the vicinity of the contact area, turns into a bi-dimensional (plane stress) divergent wave propagating in the whole target. It is the reason why the stress amplitude is expected to decline more slowly with distance (at $1/\sqrt{r}$) compared to a spherical expansion for which a decrease with distance of 1/r is observed. Accordingly, damage develops much over a greater distance in the EOI test. Thus, in the so-called open-configuration, the lateral face of the target is visualized using an ultra-high-speed camera set to framing-rates usually from between 2 µs down to 0.2 µs (Fig.16a). In this configuration, the camera is installed along the axis of the reflected light from a flash or continuous light source. The visualized surface is usually polished to increase the amount of light captured by the camera but also to improve the contrast of cracks observed.

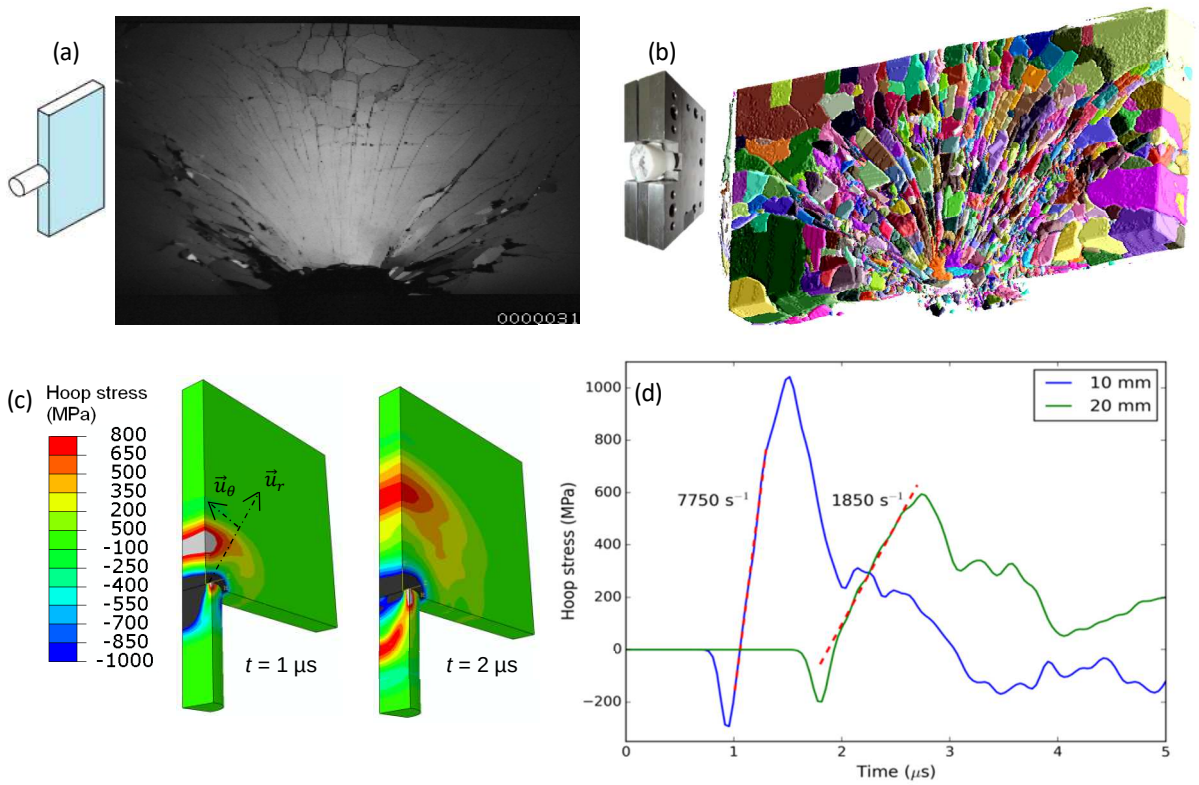

Fig. 16. The edge-on impact testing configuration. (a) EOI test conducted in open configuration and visualisation with an ultra-high-speed camera (t = 12 µs) (Forquin et al, 2018), (b) EOI test performed in sarcophagus configuration and analysis of the fragment' size distribution with X-ray micro-tomography (Forquin and Ando, 2017), (c) Numerical simulation of EOI test and (d) traces of the hoop stress at 10 mm and 20 mm from the impact point (Forquin and Ando, 2017).

In the so-called sarcophagus configuration (Fig. 16b), a metallic or polymeric casing that surrounds the ceramic tile is used to keep all the fragments in place. In order to hold the fragments in place, the target can be infiltrated after impact or kept in its transparent or opaque polymeric casing. Next, the fracture pattern can be observed post-mortem (Forquin et al, 2003b; 2018; Zinszner et al, 2015) or can be entirely scanned using X-ray tomography. A 3D segmentation algorithm can be applied in order to separate fragments in 3D allowing a particle-size distribution to be obtained (Forquin and Ando, 2017) (Fig. 2b). In the same work, the strain-rate level was analysed by a numerical calculation and was found to be about 7750 s^{-1} at 10 mm from the impact point and about 1850 s^{-1} at 20 mm from the impact point when considering an impact velocity of 175 m/s. Finally, it is observed that a single test enables the tensile damage to be explored in the impacted ceramic over a large range of strain-rates. However, this technique does not provide any direct measurements of the mechanical properties of the tested material.

As reported in chapter 4, a large number of EOI experiments have been performed with different kinds of brittle materials (ceramics, glass, concrete, ultra-high-strength concrete, rocks…). Among the most recent work conducted with ceramics one may note some other tests conducted with boron carbide (B_4C) ceramic (Strassburger et al. 2013), or with transparent ceramics such as single crystal (sapphire) and AlON (spinel) polycrystalline ceramics (McCauley et al. 2013; Forquin and Zinszner, 2017a).

14.5.2The shockless plate impact spalling test

The spalling technique based on the planar plate-impact test constitutes a convenient way to explore the tensile strength of brittle materials. As in normal plate impact, a flyer plate is projected against a target plate at an impact speed of few tens to few hundreds of m/s. However, no window plate is used on the back face of the ceramic and the flyer plate thickness is small enough compared to that of the ceramic tile so that release waves coming from the flyer and target rear faces cross each other within the ceramic. This configuration produces a tensile loading which leads to the initiation of tensile damage and dynamic fracture. The so-called spall strength (tensile strength) can be deduced by using Novikov's formula (Novikov et al, 1966) [note to PF: this Russian paper was also published in English translation; details given in the reference list]:

$$\sigma_{spall} = \frac{1}{2}\rho C_L \Delta V_{pb} \tag{9}$$

where ρ and C_L are the density and the longitudinal wave speed of the tested material and ΔV_{pb} is the pullback velocity defined as the difference between the peak velocity and the velocity at rebound measured on the sample's rear free surface. However, during a planar impact experiment, the shock loading induces a discontinuity in the stress that leads to non-homogeneous stresses and an uncontrolled strain-rate in the spall region (Forquin and Zinszner, 2017b; Dargaud and

Forquin, 2022). To overcome this limitation, a triangular-shaped compression pulse should be considered as the loading pulse applied to the target. To do so, a configuration in which a wavy-machined flyer plate is used to impact a two-layer target consisting of a buffer plate bonded to the ceramic plate (Dargaud and Forquin, 2022).

The dynamic testing facility used for the plate-impact tests and the experimental set-up are illustrated in Fig. 17. The ceramic target is stuck to a buffer on its front face. An accurate angular adjustment of the target is made to ensure that the target front face is perpendicular to the axis of the projectile. A Photon Doppler Velocimetry (PDV) system is used as the principal diagnostic system to record the particle velocity on the target rear face. The detector generates a signal that is post-processed using a sliding Fourier transform method of analysis thanks to dedicated software. By recording the beat frequency over time, a complete velocity history of the free surface is obtained (Dargaud and Forquin, 2022).

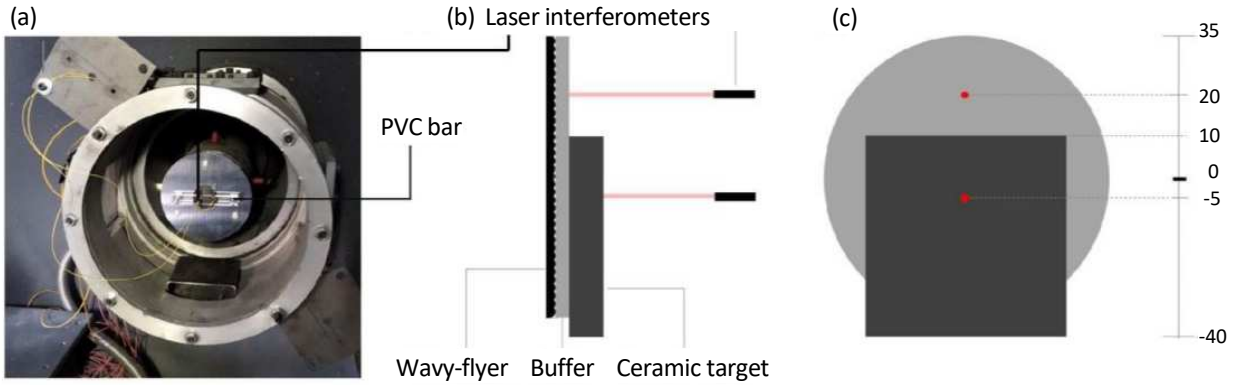

Fig. 17. (a) Instrumented rear face of the ceramic target. Schematic showing the 2 laser-probes set-up used to measure simultaneously the loading pulse and the ceramic free-surface velocity. Side view (b) and back view (c) (Dargaud and Forquin, 2022).

A specific procedure was set to identify the strain-rate corresponding to the ceramic tensile failure. The procedure consists in simulating the experiment by considering the loading applied to the ceramic. To do so, the velocity at the buffer backside is measured by using a second optical probe in addition to the probe directed to the rear face of the ceramic target (Figs. 17 b, 17c). This particle velocity provides the loading pulse transferred to the ceramic according to the following equation:

$$\sigma_{transmitted} = \frac{\rho C_L \times \rho_b C_b}{\rho C_L + \rho_b C_b} V_b \tag{10}$$

where ρC_L is the acoustic impedance of the target, $\rho_b C_b$ is the acoustic impedance of the buffer and V_b is the buffer's free-surface velocity. This pulse is used as input data in the numerical simulation.

Several flyer plate geometries and nominal impact speeds were considered in an experimental campaign applied to SiC ceramic (Fig. 18a). Wavy-machined flyer plates produced by chip-forming with a wave shape profile of height 0.125-0.25 mm and half-periods between 0.5 to 1 mm were launched at a nominal impact velocity ranging from 200 to 450 m/s. The spall strength of the target was deduced from the Novikov formula that is based on the measurement of the particle velocity on the rear face of the ceramic target. The main results obtained with Hexoloy SiC ceramic are reported in Fig. 18b in terms of dynamic tensile strength versus the applied strain-rate. The results are in excellent agreement with those measured using the GEPI technique on the same material Hexoloy SA (Zinszner et al, 2017).

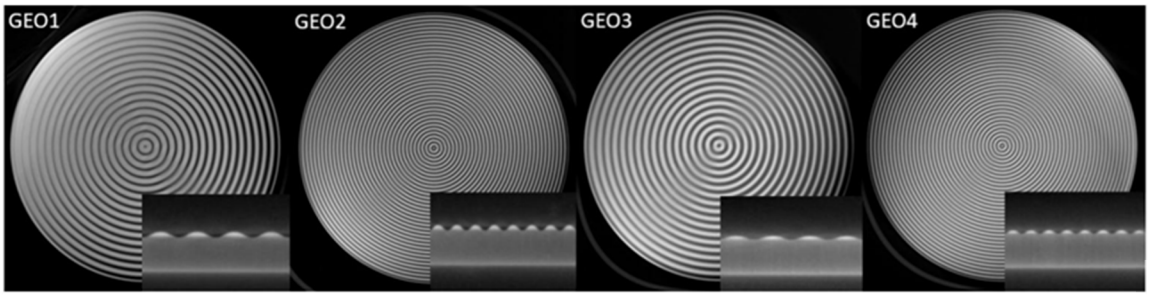

(a)

Flyer geometry	Profile period (mm)	Profile height (mm)	Nominal impact velocities (m/s)		
GEO1	1	0.25	350	-	-
GEO2	0.5	0.25	-	250	200
GEO3	1	0.125	350	-	-
GEO4	0.5	0.125	350	450	450

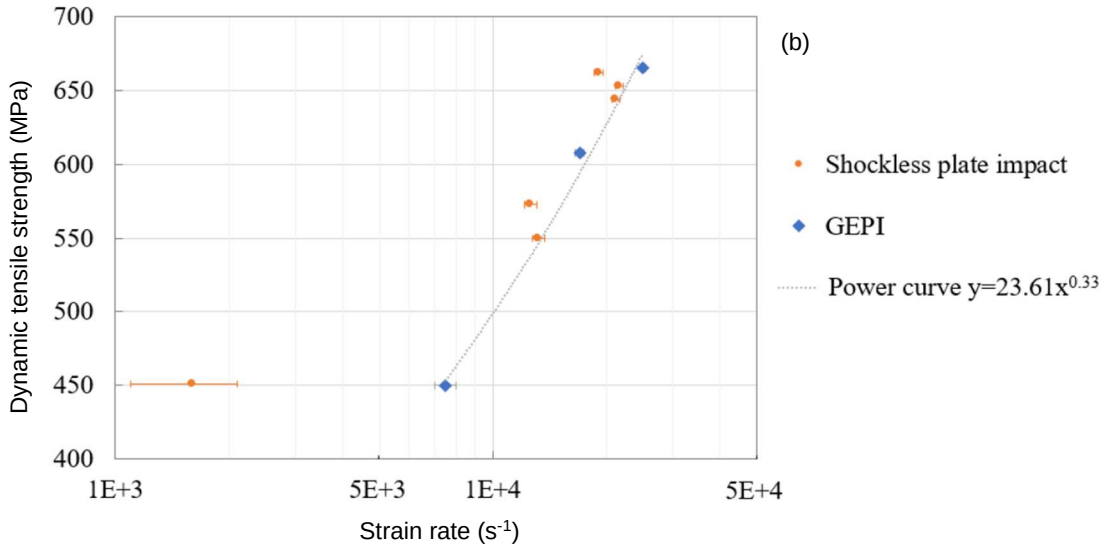

Fig. 18. Shockless plate-impact experiments (Dargaud and Forquin, 2022). (a) Flyer plate geometries and nominal configurations. (b) Spall strength of Hexoloy as function of the applied strain-rate and comparison with GEPI experimental results from Zinszner et al (2017).

14.5.3 Synthesis: experimental methods to characterise the tensile response of ceramics

A short summary of the main experimental methods considered to characterise the tensile behaviour of ceramics is proposed in Fig. 19. Their main advantages and drawbacks are listed in Table 5. As previously stated, dynamic bending or Brazilian tests conducted by means of SHPB apparatus are limited to strain-rates not exceeding a few hundreds of s^{-1} to ensure correct mechanical equilibrium of the sample. EOI experiments are recommended to investigate the fragmentation process in ceramics by means of ultra-high-speed imaging or post-mortem observations (sarcophagus configuration). However, the level of strain-rates usually ranges from a thousand to ten thousand of s^{-1}. Standard planar plate-impact can provide a measurement of spall strength at very high strain-rate by applying Novikov's formula. However, due to discontinuity in the stress field, the loading-rate is difficult to establish. Finally, spalling experiments conducted with shockless plate-impact or GEPI facility provide a better characterisation of the tensile strength at controlled strain-rates in the range (1000 – 30 000 s^{-1}). However, post-mortem analysis of the target is not an easy task due to the dispersion of fragments at failure.

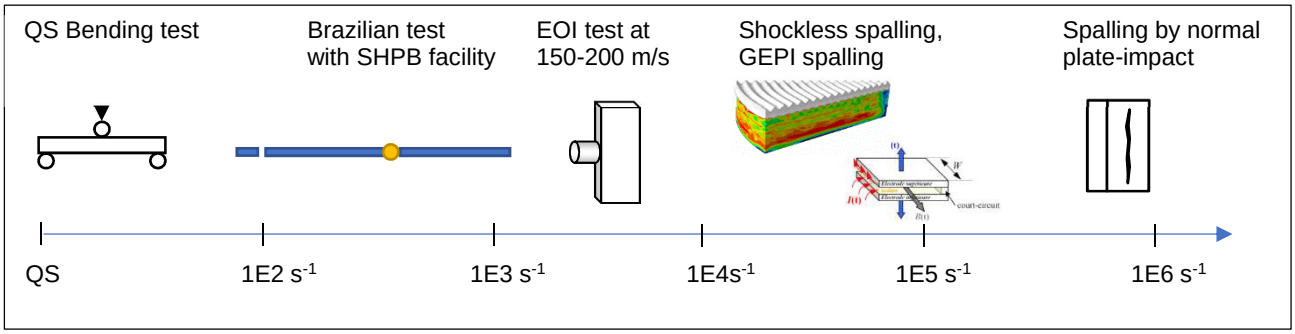

Fig. 19. Orders of magnitude of the strain-rate reached in samples subjected to various tensile loading tests.

Table. 5. Some advantages and drawbacks of testing methods use to characterize the tensile behaviour of ceramics.

Techniques	Advantages	Drawbacks
Dynamic bending tests or Brazilian tests	Single fragmentation: characterisation of the flaw distribution (Weibull parameters)	- Low strain-rate
Standard spalling test by normal plate-impact	Dynamic strength measurement	- Non-controlled strain-rate, - Non-uniform stress field
Spalling by GEPI	Dynamic strength vs strain-rate, post-mortem analysis at low rate	- Imposed rising time, - No visualization of damage
Spalling by shockless plate-impact	Controlled and constant strain-rate, more homogeneous stress field	- Post-mortem analysis difficult, - No visualization of damage
Edge-on impact tests in open and sarcophagus configurations	Convenient and cheap, visualisation of damage with ultra-high-speed imaging, X-ray tomography analysis	- No strength measurement - Limited range of strain-rate

14.6 Fragmented ceramics under impact loadings

The ballistic impact of an armour piercing projectile against a bilayered configuration produces a fragmentation process in the ceramic tile that develops in a few microseconds. However, the projectile penetration process lasts more than 20 to 30 microseconds. During this loading stage, the projectile penetrates damaged ceramic. This is the reason why the mechanical behaviour of fragmented ceramic may play an important role in the penetration resistance of the armour and needs to be investigated. To do so, a so-called tandem configuration that consists of a double-impact test was developed in the 3SR Lab. (Zinszner et al, 2015; Duplan and Forquin, 2021). In the first stage, a normal impact test is performed against a sandwich configuration composed of a thin steel plate 1 mm thick as the front face, an aluminium plate as backing and a ceramic tile in the centre of the target (Fig. 20a). Four small (few mm²) pieces of steel sheet 0.1 mm thick are placed between the ceramic and the backing at each corner to ensure a constant gap between both plates (Zinszner et al, 2015). This produces an impedance discontinuity leading to a more intense fragmentation process in the ceramic tile. The sandwich is inserted into a sarcophagus to prevent any loss of fragments during and after the first impact. This first stage consists in the impact of a cylindrical projectile, 10 mm in diameter and 15 mm in length, hitting the target with an impact speed of about 175 m/s. An example of the damage pattern induced by such an impact is illustrated in Fig. 20b.

After this first shot, a second impact is performed in order to analyse the residual behaviour of the fragmented ceramic. To do so, the front side of the sarcophagus as well as the confinement steel plate are removed. A conical nose projectile made of steel, 16.7 mm in length, 10 mm in diameter is used to impact the fragmented ceramic. An example of pictures recorded using an ultra-high-speed camera showing the interaction between the projectile and the ceramic as well as the final ejection of fragments is given in Fig. 20c. In addition, the particle velocity on the rear surface of the aluminium plate was recorded using a laser interferometer. For instance, two SiC ceramics named (PS-S and PS-L) were subjected to the tandem (normal impact + penetrating impact) test configuration. As demonstrated by Forquin et al (2018), due to different distributions of flaws, the PS-L ceramic was observed to generate much larger fragment sizes in normal impact stage than the PS-S ceramic, as illustrated in Fig. 21a. Next, both ceramics were subjected to penetrating impact and the velocity profile of the aluminium plate was measured (Fig. 21b). In the case of the fragmented PS-L ceramic, the velocity quickly rose in the first microsecond and then rose more slowly after a few tens of microseconds. In the case of the fragmented Hexoloy, the velocity rise was more continuous until 25 µs. These curves demonstrate that the fragmented PS-L presents a higher residual resistance in the first few microseconds of impact. Finally, as postulated by Krell and Strassburger (2004) (cf. section 14.2), lower ceramic fragmentation (i.e. larger fragment size) increases the dwell time on the ceramic surface before its penetration and provides better resistance of the fragmented ceramic during the penetration stage. In addition, ballistic impact with the same projectile design was performed against an aluminium tile without the presence of fragmented ceramic (Fig. 21b). This showed a lower level of velocity during the first 5 microseconds than with fragmented ceramic present. Again, it demonstrates the high resistance of fragmented ceramics to penetration in the first few microseconds of the penetration stage.

These experimental measurements can be used to identify by an inverse approach (i.e. successive comparison between experimental data and numerical predictions) the parameters of a constitutive model describing the dynamic behaviour of the fragmented ceramic, such as the Johnson-Holmquist model when the damage variable is set to one. This model is briefly introduced in the following subsection.

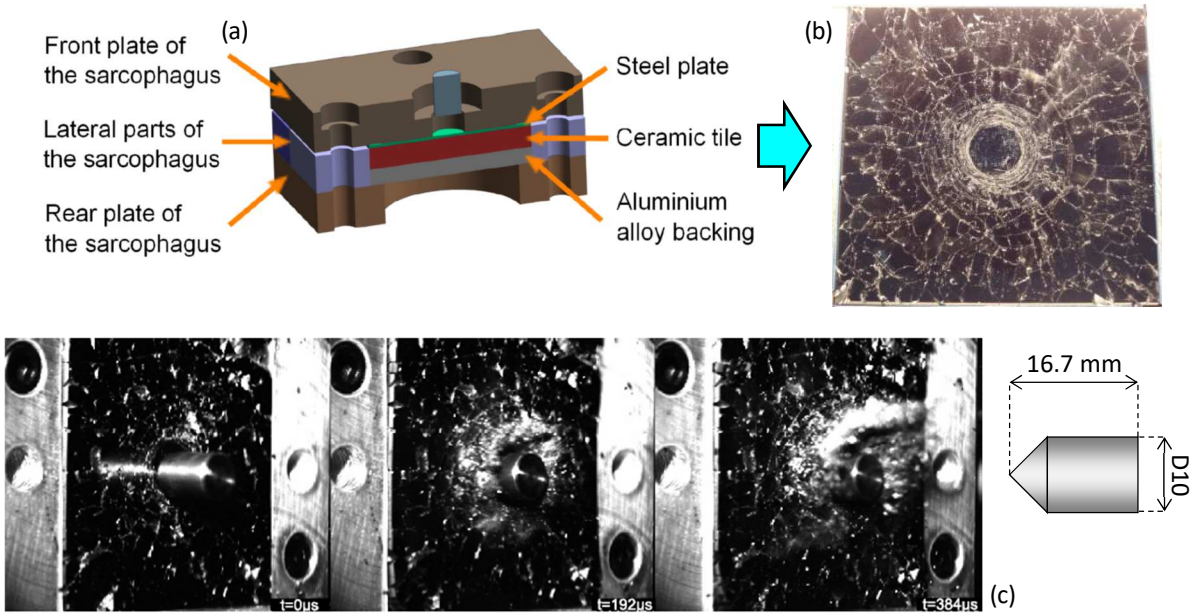

Figure 20. The tandem testing technique (Zinszner et al, 2015). (a) Normal impact against a sandwich configuration composed of a steel front plate, a ceramic tile and an aluminium backing plate. (b) Top view of the ceramic after normal impact. (c) Second impact with a conical-nose projectile at an impact speed of 175 m/s.

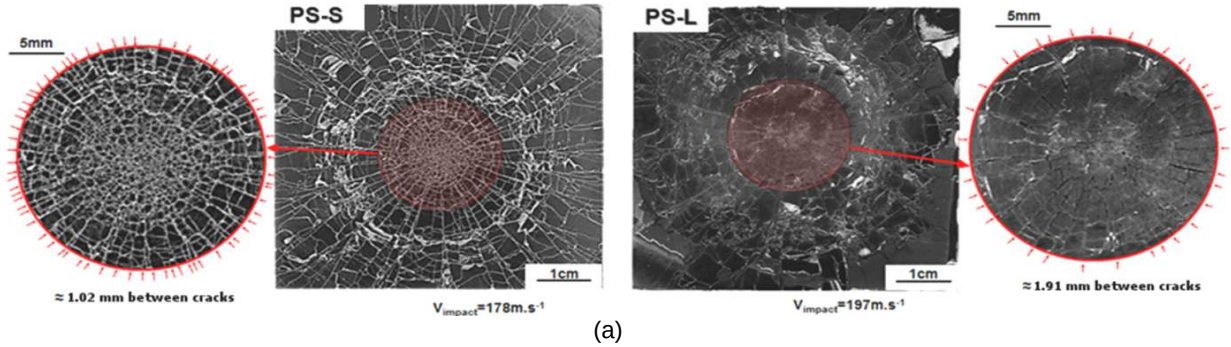

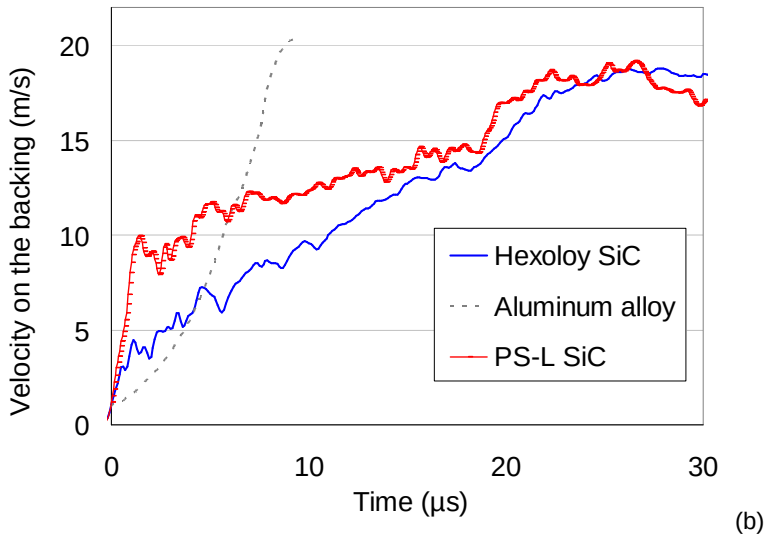

Fig. 21. Tandem impact experiments performed with two SiC ceramics. (a) Observation of damage after normal impact tests (Forquin et al, 2018). (b) Velocity profile measured in penetration test with both ceramics.

14.7 Introduction to the Johnson-Holmquist material model for ceramics under ballistic impact

The study of the impact behaviour of ceramic materials through numerical simulation requires a proper material model. The models proposed by Johnson and Holmquist are the ones most used to simulate armour ceramics. Other ceramic material models can be used as well, such as the model by Simha (1998) or the more general Kayenta model (Brannon et al, 2009). All these models are phenomenological softening plasticity models, with variations in their formulations of strength and failure. These phenomenological models do not describe the true microscopical failure mechanisms, but provide the response of the material given a loading condition. The advantage of these models is that they can easily capture the response, without having to know the true underlying damage and plasticity mechanisms.

The Johnson and Holmquist model, available in three versions generally referred to as JH-1 (Johnson and Holmquist, 1990), JH-2 (Johnson and Holmquist, 1994) and JHB (Johnson-Holmquist-Bessel, Johnson et al. (2003)) is one of the most common and widely used models for simulations of the behaviour of ceramic materials subjected to extreme loadings in terms of pressure and high strain rate. This model describes the essential aspects of the behaviour of brittle materials under confinement based on a polynomial equation of state, on a plasticity envelope reproducing the increase in resistance with the confinement pressure and the growth of damage in the material. For the plasticity envelope (as for the equation of state) two curves are defined, one corresponding to the undamaged material, the other describing the behaviour of the totally fragmented ceramic.

In the case of the JH2 model, the plasticity envelope of the intact material is described by the relation:

$$\sigma_i^* = A(P^* + T^*)^n(1 + C ln\, \dot{\varepsilon}) \tag{10}$$

where σ_i^* is the normalized equivalent stress (relative to the HEL equivalent stress), P^* is the normalized pressure (relative to the hydrostatic pressure at the HEL) and the value of T^* corresponds to the normalized pressure ((also relative to the hydrostatic pressure at the HEL) for which the equivalent stress is zero. The envelope of plasticity of the fractured material is described by

$$\sigma_f^* = B(P^*)^m(1 + C ln\, \dot{\varepsilon}) \tag{11}$$

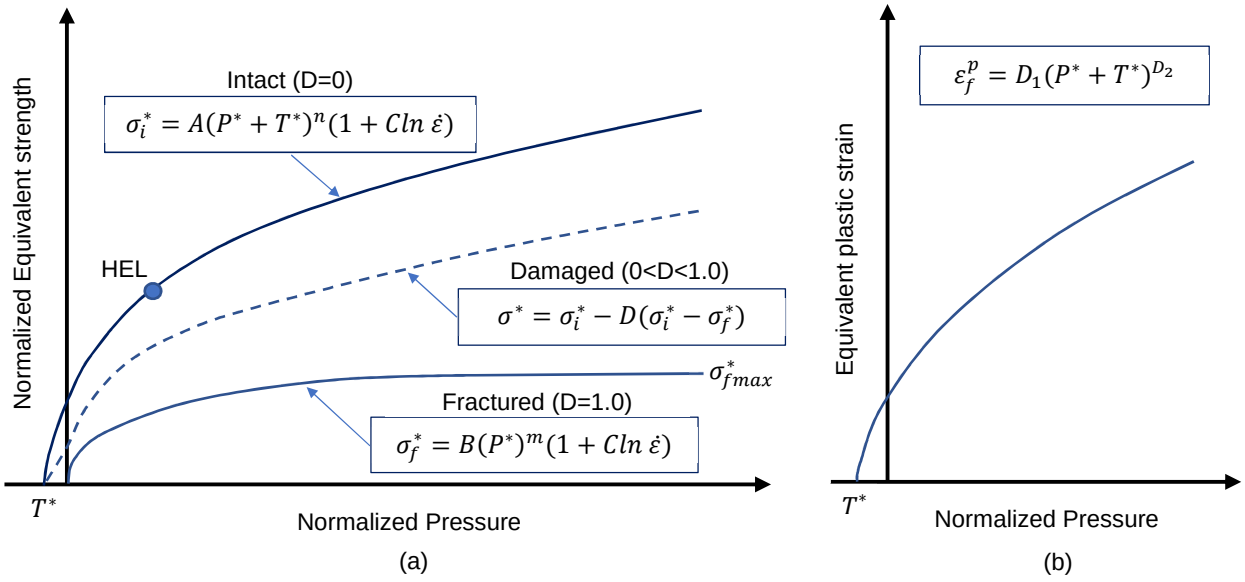

Fig. 22. The JH-2 plasticity-damage model. (a) Envelopes of intact and fractured material, (b) Damage evolution law.

The damage evolution law, based on the increments of plastic strain (which can be either compression or tension), is used as an interpolation variable between the intact and the fractured behaviour.

$$D = \sum \frac{\Delta\varepsilon^p}{\varepsilon_f^p} \quad , \tag{12}$$

with

$$\varepsilon_f^p = D_1(P^* + T^*)^{D_2} \quad (13)$$

So, the strength of the material is calculated whatever the level of damage.

$$\sigma^* = \sigma_i^* - D(\sigma_i^* - \sigma_f^*) \quad (14)$$

However, although these equations make it possible to consider the transition of the behaviour of a material between its intact and fully fragmented state, the modelling of the behaviour of the fragmented material itself remains crude and does not consider a specific formulation for tensile damage. In addition, the absence of a microstructural parameter also prevents precise modelling of the differences in ballistic behaviour observed between different grades of silicon carbide. Indeed, some model constants can only be determined using an inverse approach by performing numerical simulations of impact tests. This is one of the biggest disadvantages of these models. It should also be noted that although sensitivity to the strain-rate of the compressive strength of the material is taken into consideration , JH models maintain a constant ultimate hydrostatic tensile strength up to the point of full failure at which point there is a sudden collapse to zero strength. However, experimentally the tensile strength of ceramics is known to be strongly sensitive to strain-rate and dynamic failure is a progressive process driven by crack inception and propagation. Finally, coupling between tensile damage models to softening plasticity models should constitute a main topic for further research.

14.8 Conclusions

Although ceramic materials are widely used in very high-strain-rate loading conditions (such as in armour systems) the relationship between their microstructure and their ballistic efficiency remains difficult to establish. The main reason is that, when a bilayer or multilayer configuration made with an armour ceramic as front face is subjected to the impact of an Armour Piercing (AP) projectile, very complex transient and successive dynamic loading develops within the ceramics inducing complex and intense damage and deformation processes that are not observed in classical quasi-static testing such as bending or uniaxial compression tests. Indeed, ballistic impact against a ceramic armour leads to different loading stages applied to the ceramic that can be separated as: dynamic triaxial compression of the virgin material, which leads to microplasticity coupled to microcracking mechanisms; high strain-rate tensile loadings, which generates a dense network of oriented cracks (the so-called multiple fragmentation process) initiated on defects distributed within the microstructure (sintering flaws, pores, heterogeneities…). These damage and deformation stages are followed by the penetration process of the projectile or its debris through the fragmented media. In this stage, the previous state of damage of the ceramic is supposed to play a major role as a lower cracking density is supposed to increase the dwell time of the projectile on the ceramic surface and to increase the subsequent abrasive efficiency of the ceramic fragments.

As illustrated in the present chapter, various techniques have been applied to ceramics to explore their high-strain-rate behaviour. One may distinguish the specific techniques that enable the analysis of the damage mechanisms in view of better understanding the role plaid by microstructural parameters. The edge-on impact test figures amongst these. It can be performed in either the open or sarcophagus configuration, enabling the generation of high strain-rate tensile loading. Time resolved observations can be made by using an ultra-high-speed camera set to high recording frequencies. Post-mortem observations can be conducted by using X-ray microtomography. The pyrotechnic spherical expansion test is another method to explore the microplasticity (TEM observations) and microcracking (SEM observations) modes under high triaxial loadings and stresses largely exceeding the HEL of the ceramic.

Other techniques have been developed to get a direct measurement of the mechanical response of ceramics at very high rates. Spalling produced by planar plate impact figures amongst these. It allows characterisation of the spall (tensile) strength. However, spalling tests by shockless plate-impact or HPP High-Pulsed Power technologies allow much better control of the level of strain-rate applied to the target, making it possible to exploring the sensitivity of ceramics' tensile strength to strain-rate. The compressive mechanical response of ceramics is not well characterised by the uniaxial compression test, as sample failure may result from induced tensile stresses and also uniaxial compression loading is not representative of ballistic impact. Triaxial tests give access to the increase of strength with pressure but in a limited range of pressure. Finally, planar plate-impact and HPP apparatus, instrumented with laser interferometry or pressure gauges, provides characterisation of the HEL (Hugoniot Elastic Limit) and of the mechanical strength and Hugoniot state of the ceramic under very high pressures but in a limited range of plastic strain.

Among the most important findings, one may note that under tensile loading, ceramics undergo a change of behaviour from a probabilistic and size-dependent response in static (single fragmentation) to a deterministic and strain-rate-dependent response at high strain-rates (multiple fragmentation). Under compression, as shown in triaxial tests, a transition from a brittle to a ductile response occurs with the increase of confining pressure. Moreover, microstructural parameters related to the applied sintering or manufacturing process are seen to play an important role by influencing the cracking and deformation modes at the microscale and the mechanical behaviour of ceramics at the macroscale. Several constitutive laws have been proposed in the literature to model the influence of pressure and strain-rate on the mechanical behaviour of ceramics. However, constitutive models that better describe the coupling effects (tensile damage/plastic strain driven damage) and the influence of microstructural parameters still need to be developed and validated in order to better numerically simulate the mechanical response of armour ceramics under ballistic impact.

Acknowledgements:

The author gratefully acknowledges the proofreading of the chapter by Dr. S. Walley.

References:

Barron E.R., Alesi A.L., Park A.F. (1969) Body armor for aircrewmen. Tech. Rep. 69-43-CE, U.S. Army Natick Laboratories

Bless S.J., Ben-Yami N., Apgar L. Eylon D. (1992) Impenetrable targets struck by high velocity tungsten long rod. Proc. 2nd Int. Conf. on Structures under Shock and Impact, Portsmouth, UK, pp. 27-38

Bourne N., Millet J., Pickup I. (1997) Delayed failure in shocked silicon carbide. J. Appl. Phys. 81, 6019–2023

Brannon R., Fossum A., Strack O. (2009) Kayenta: theory and user's guide, Tech. Rep. SAND2009-2282 (Sandia National Laboratories), Albuquerque, NM.

Cagnoux J., Chartagnac P., Hereil P.-L. (1987) Lagrangian analysis: a modern tool of the dynamics of solids. Ann. Phys. Fr., 12, 514–541.

Chen J.J., Guo B.Q., Liu H.B., Liu H., Chen P.W. (2014) Dynamic Brazilian Test of Brittle Materials Using the Split Hopkinson Pressure Bar and Digital Image Correlation Strain, 50, 563–570

Cosculluela A. (1992) Plasticité, endommagements et ruptures des alumines sous sollicitations dynamiques triaxiales : influence de la taille des grains (Ph.D. dissertation), University of Bordeaux, France.

Cosculluela, A., Forquin, P. (2022) Damage in Armor Ceramics Subjected to High-Strain-Rate Dynamic Loadings: The Spherical Expansion Shock Wave Pyrotechnic Test. In: Voyiadjis, G.Z. (ed.) Handbook of Damage Mechanics. Springer, New York, NY. https://doi.org/10.1007/978-1-4614-8968-9_81-1

Danzer R., Borger A., Fellner M. (2009) Evolution of defects in pressed and sintered electro-ceramic components. In 27th Annual Cocoa Beach Conference on Advanced Ceramics and Composites-B, volume 270, page 343. John Wiley & Sons, 2009.

Dargaud M. (2021) Experimental and numerical analysis of the failure modes induced in ceramic materials under dynamic loading. (Ph.D. dissertation), Université Grenoble Alpes, France.

Dargaud M., Forquin P. (2022) A Shockless Plate-Impact Spalling Technique Based on Wavy-Machined Flyer-Plates to Evaluate the Strain-Rate Sensitivity of Ceramic Tensile Strength, J. Dynamic Behavior Mat., 8, 73–88. DOI: 10.1007/s40870-021-00317-4.

den Reijer P.C. (1991) Impact on ceramic faced armour. PhD dissertation, Technical University of Delft

Deng H., Nemat-Nasser S. (1992) Dynamic damage evolution in brittle solids. Mechanics of materials, 14(2):83–103.

Dunlay W.A., Tracy C.A., Perrone P.J. (1989). A Proposed Unaxial Compression Test for High Strength Ceramics. MTL TR 89-89, U.S. Army Materials Technology Laboratory, Watertown (Massachussets). Final Report.

Duplan Y., Forquin P. (2021) Investigation of the multiple-fragmentation process and post-fragmentation behaviour of dense and nacre-like alumina ceramics by means of tandem impact experiments and tomographic analysis, Int. J. Impact Eng., 155, 103891, DOI: 10.1016/j.ijimpeng.2021.103891.

Evans A.G. (1974) Slow crack growth in brittle materials under dynamic loading conditions. International Journal of Fracture 10 (2), 251-259.

Feng R., Raiser G.R., Gupta Y.M. (1998). Material strength and inelastic deformation of silicon carbide under shock wave compression. J. Appl. Phys. 83 (1), 79–86

Forquin P. (2003) Endommagement et fissuration de matériaux fragiles sous impact balistique, rôle de la microstructure. Ph.D. dissertation, Ecole Normale Supérieure de Cachan, France.

Forquin P. Zinszner J.L. (2017a) Experimental Study of the Dynamic Fragmentation in Transparent Ceramic Subjected to Projectile Impact. In: Casem D., Lamberson L., Kimberley J. (eds) Dynamic Behavior of Materials, Volume 1, pp 165-170, DOI: 10.1007/978-3-319-41132-3_23. Book series: Proceedings of the Society for Experimental Mechanics Series. Springer

Forquin P., Ando E. (2017) Application of micro-tomography and image analysis to the quantification of fragmentation in ceramics after impact loading. Phil. Trans. R. Soc. A. 375(2085), 20160166.

Forquin P., Blasone M., Georges D., Dargaud M. (2021) Continuous and discrete methods based on X-ray computed-tomography to model the fragmentation process in brittle solids over a wide range of strain-rates-application to three brittle materials, J. Mechanics and Physics of Solids, 152, 104412, DOI: 10.1016/j.jmps.2021.104412.

Forquin P., Denoual C., Cottenot C.E., Hild F. (2003a). Experiments and Modelling of the Compressive Behaviour of two SiC Ceramics. Mechanics of Materials. 35, 987-1002.

Forquin P., Hild F. (2010) A probabilistic damage model of the dynamic fragmentation process in brittle materials. Advances in Applied Mech, Giessen & Aref Eds., 44:1-72. Academic Press, San Diego, CA.

Forquin P., Metzen L., Lachaume F., Zavard M., Charrier P., Genevois J., Margossian A. (2022) Analysis of damage in two-layer ceramic-UHMWPE armour under multi-hit loading from API-BZ projectile impact, Light-Weight Armour for Defence & Security, Freiburg, Germany

Forquin P., Tran L., Louvigné P-F., Rota L., Hild F. (2003b) Effect of Aluminum Reinforcement on the Dynamic Fragmentation of SiC Ceramics. Int. J. Impact Eng., 28:1061-1076.

Forquin P., Zinszner J.-L. (2017b) A pulse-shaping technique to investigate the behaviour of brittle materials subjected to plate-impact tests. Phil. Trans. R. Soc. A 20160333. DOI: 10.1098/rsta.2016.0333.

Forquin P., Zinszner J.-L., Rossiquet G., Erzar B. (2018) Microstructure influence on the fragmentation properties of dense silicon carbides under impact. Mech. Mat., 123:59-76.

Forquin P., Cosculluela A. (2022) Damage in Armor Ceramics Subjected to High-Strain-Rate Dynamic Loadings: The Edge-on Impact Test. In: Voyiadjis, G.Z. (ed.) Handbook of Damage Mechanics. Springer, New York, NY. https://doi.org/10.1007/978-3-030-60242-0_94

Forquin, P., Blasone, M., Georges, D., Dargaud, M., Saletti, D., Andò, E., 2020. The Brittle's CODEX chair, DYMAT Winter School 2020, in Les Houches School of Physics, France.

Gooch W.A. (2011) Overview of the development of ceramic armor technology: Past, present and in the future. Advances in Ceramic Armor 7, New York, Wiley, 195-213.

Grady. D. (1994) Shock-wave strength properties of boron carbide and silicon carbide. Journal de Physique IV, Proceedings, EDP Sciences, 1994, 04 (C8), pp.C8-385-C8-391. 10.1051/jp4:1994859. jpa-00253419.

Hayun S. (2017) Reaction-bonded boron carbide for lightweight armor: the interrelationship between processing, microstructure, and mechanical properties. American Ceramic Society Bulletin, 96(6):20–6.
Heard H.A., Cline C.F. (1980) Mechanical Behaviour of Polycrystalline BeO, Al2O3 and AlN at High Pressure. J. Mater. Sci. 15, 1889-1897.
Johnson G.R., Holmquist T.J. (1990) A Computational Constitutive Model for Brittle Materials Subjected to Large Strains, High Strain Rates and High Pressures, in Proceedings of the EXPLOMET Conference (San Diego, 1990).
Johnson G.R., Holmquist T.J. (1994) An improved computational constitutive model for brittle materials, AIP Conference Proceedings 309, 981.
Johnson G.R., Holmquist T.J., Beissel S.R. (2003) Response of aluminum nitride (including a phase change) to large strains, high strain rates, and high pressures, Journal of Applied Physics 94, 1639.
Kipp M.E., Grady D.E. (1990) Shock Compression and Release in High-Strength Ceramics. Shock Compression of Condensed Matter. ed. Schmidt S. C., Johnson, J.N., Davidson, L.W., Elsevier Science Publishers B.V.
Krell A., Strassburger E. (2014) Order of influences on the ballistic resistance of armor ceramics and single crystals. Materials Science and Engineering: A, 597:422–430.
Lankford J. (1977) Compressive strength and microplasticity in polycristalline alumina. Journal of Materials Science 12, 791-796.
Lankford J. (1981) Temperature-strain rate dependence of compressive strength and damage mechanisms in aluminium oxide. J. Mater. Sci. 16, 1567-1578.
Lankford J. (1991) The compressive strength of strong ceramics: microplasticity versus microfracture. J. Hard Materials 2 (1-2), 55-77.
LaSalvia J.C., Leavy R.B., Houskamp J.R., Miller H.T., MacKenzie D.E., Campbell J. (2009) Ballistic impact damage observations in a hot-pressed boron carbide. In Ceramic Engineering and Science Proceedings, volume 30, page 45.
LaSalvia J.C., McCauley J.W. (2010) Inelastic deformation mechanisms and damage in structural ceramics subjected to high-velocity impact. International journal of applied ceramic technology, 7(5):595–605.
Lindl, J. (1995) Physics of Plasmas, 2, 3933. https://doi.org/10.1063/1.871025
Madhu V., Ramanjaneyulu K., Balakrishna Bhat T., Gupta N.K. (2005). An experimental study of penetration resistance of ceramic armour subjected to projectile impact. Int. J. Impact Eng. 32, 337–350
Malaise F. (1999). Réponse d'une céramique à l'impact d'un barreau à grande vitesse (1500 m/s). Croisement essais dynamiques-modélisation numérique. PhD thesis, Ecole Nationale Supérieure d'Arts et Métiers, Centre de Bordeaux, (in french).
Mangeant C., Lassalle F., L'Eplattenier P., Hereil P.L., Bergues D., Avrillaud G. (2002) Syrinx project: HPP generators devoted to isentropic compression experiments, AIP conference proceedings, Shock Compression of Condensed Matter 2001, 1173-1176.
McCauley, J.W., Strassburger, E., Patel, P., Paliwal, B., Ramesh, K.T. (2013) Experimental Observations on Dynamic Response of Selected Transparent Armor Materials. Experimental Mechanics, 53, 3-29.
Meyers M.A. (1994) Dynamic behavior of materials. John Wiley & Sons Inc., Canada
Novikov S.A., Divnov I.I., Ivanov A.G. (1966) Failure of steel, aluminium and copper under explosive loading. Physics Metals Metallography, 21(4), 122-128
Reddy P.R.S., Savio S.G., and Madhu V. (2020) Ceramic composite armour for ballistic protection. Handbook of Advanced Ceramics and Composites: Defense, Security, Aerospace and Energy Applications, 357–402.
Roberson C.J. (1995) Ceramic materials and their use in lightweight armour systems. In: Lightweight armour system symposium. Royal Military College of Science, Cranfield, England.
Rosenberg J., Yaziv D., Yeshurun Y., Bless S.J. (1987) Shear strength of shock-loaded alumina is determined with longitudinal and tranverse mangafin gauge. J. Appl. Phys. 62 (3), 1120-1122.
Rossiquet G. (2012) Carbure de silicium pour application blindage : élaboration et étude du comportement à l'impact, (Ph.D. dissertation), Université de Bourgogne, France.
Scapin M., Peroni L., Avalle M. (2017) Dynamic Brazilian Test for Mechanical Characterization of Ceramic Ballistic Protection. Hindawi, Shock and Vibration, Vol. 2017, Article ID 7485856
Shockey D.A., Marchand A.H., Skaggs S.R., Cort G.E., Burkett M.W., Parker R. (1990) Failure phenomenology of confined ceramic targets and impacting rods. International Journal of Impact Engineering, 9(3):263–275, 1990.
Simha C. (1999) Arbor Ciencia Pensamiento Y Cultura, Ph.D. thesis, University of Texas [question to PF: should this be Simha C.H.M. (1998) "High rate loading of a high purity ceramic: 1D stress experiments and constitutive modeling", PhD thesis, University of Texas at Austin]
Strassburger E., Hunzinger M., Patel P., McCauley J.W. (2013) Analysis of the fragmentation of AlON and Spinel under ballistic impact, J. Appl. Mech. 80, 031807
Taylor K. and Palicka R. (1974) Dense carbide composite bodies and method of making same, March 12 1974. US Patent 3,796,564.
Zinszner J.-L., Erzar B., Forquin P. (2017) Strain-rate sensitivity of the tensile strength of two silicon carbides: experimental evidence and micromechanical modelling, Phil. Trans. R. Soc. A, 375(2085), 20160167
Zinszner J-L, Forquin P, Rossiquet G (2015) Experimental and numerical analysis of the dynamic fragmentation in a SiC ceramic under impact. Int J Impact Eng 76:9–19